ABSTRACT

Leah B. Fuller. DIAGENETIC ALTERATION OF FORAMINIFERAL TESTS IN QUATERNARY SEDIMENTS, FRYING PAN PHOSPHATE DISTRICT, ONSLOW BAY, NORTH CAROLINA. (Under the direction of Dr. Scott W. Snyder) Department of Geology, May 2004.

Significant phosphate deposits have been documented in the Miocene Pungo River Formation and the Quaternary sands of southern Onslow Bay, North Carolina (Frying Pan phosphate district). Foraminifera collected from the Quaternary sands were visually assessed to show various degrees of diagenetic alteration that appear to correlate in areal distribution with phosphate concentrations in the underlying Miocene and surface Quaternary sediments.

Populations of high-magnesium (> 4% Mg) miliolid foraminifera from the Frying Pan phosphate district were analyzed using proton induced x-ray emission (PIXE) spectrometry, a multi-elemental analysis technique, to determine chemical signatures for the population. Results from these analyses confirm that the diagenetic alteration is largely a process of ferruginization – iron concentrations in samples analyzed ranged from 0% to 9.8% Fe. Visual assessments of degree of alteration parallel the iron concentrations in foraminiferal tests. The iron signatures of the samples served as a basis to investigate the relationship between the areal distribution of phosphorites in the Miocene and Quaternary sediments with the diagenetic alteration in foraminifera.

There is no simple spatial relationship between ferruginization of Quaternary foraminifera and the lithology/mineralogy of the immediately underlying Miocene

sediments in the Frying Pan phosphate district. In general, the highest Fe signatures are produced by foraminiferal samples collected from cores that penetrated the area of highest phosphate concentration (seismic units FPS-1 and FPS-2 inside the FPH 3% P_2O_5 contour). Samples collected from Quaternary sands overlying the foraminiferal quartz sand unit (FPS-6), and those collected from the northern extent of the phosphate district, contained the lowest Fe concentrations.

Comparison of iron concentrations in foraminifera to geochemical data for the phosphatic units of the Miocene Pungo River Formation and Quaternary sands suggests that the ferruginization of the foraminifera is related to the iron component of the phosphate pellets. Another likely source of iron is iron minerals in the mud of the fourth-order seismic sequences FPS-2 and FPS-3.

In the Frying Pan phosphate district, the Quaternary high-Mg miliolid foraminiferal tests undergo ferruginization that is likely related to the replacement of Mg by Fe^{+2} leached (by groundwater) from iron sulfides (e.g., pyrite) in the underlying Miocene phosphate grains, and perhaps also iron oxides in the mud facies.

DIAGENETIC ALTERATION OF FORAMINIFERAL TESTS IN QUATERNARY SEDIMENTS, FRYING PAN PHOSPHATE DISTRICT, ONSLOW BAY, NORTH CAROLINA

A Thesis

Presented to

the Faculty of the Department of Geology

East Carolina University

In Partial Fulfillment

of the Requirements for the Degree

Master of Science in Geology

by

Leah B. Fuller

May 2004

DIAGENETIC ALTERATION OF FORAMINIFERAL TESTS IN QUATERNARY SEDIMENTS, FRYING PAN PHOSPHATE DISTRICT, ONSLOW BAY, NORTH CAROLINA

by
Leah B. Fuller

APPROVED BY:

DIRECTOR OF THESIS _____
Scott W. Snyder

COMMITTEE MEMBER _____
Richard Mauger

COMMITTEE MEMBER _____
Terri Woods

COMMITTEE MEMBER _____
Larry H. Toburen

COMMITTEE MEMBER AND CHAIRMAN OF THE DEPARTMENT OF GEOLOGY

_____
Stephen J. Culver

DEAN OF THE GRADUATE SCHOOL

_____
Paul Tschetter

ACKNOWLEDGMENTS

Funding for this study was provided in part by a grant from the Cushman Foundation for Foraminiferal Research. In addition, facilities were graciously provided me by the Central Environmental Laboratory (CEL) and the East Carolina University Accelerator Laboratory (ECUAL), located on the campus of East Carolina University.

I am eternally grateful to Dr. Scott W. Snyder for offering this project to me and directing its course. I thank Dr. Larry Toburen for welcoming a geologist into his nuclear physics world, being persistently patient with my physics ignorance, and for persevering despite all. I thank the members of my committee: Dr. Richard Mauger, who spent hours bringing concepts of physics and chemistry down to my level – his edits and insight were invaluable; Dr. Terri Woods, for keeping me on the path; and Dr. Stephen J. Culver, for his editing time, his dry humor and hilarious stories, and indispensable advice. Drs. Shinpaugh and Justiniano, and the staff and students of ECUAL were very open to the collaboration, and were always available for me. I thank Deborah Daniel for allowing me to invade her laboratory for months on end, mixing my volatile chemicals and answering my most inane chemistry questions.

Because some of my best experiences at East Carolina University involved teaching, I want to thank the people who made it possible: Dr. Stephen Harper for giving me my start and encouraging my interest, Drs. Donald Neal and Stephen J. Culver allowed me to assist in teaching upper-level courses with enthusiastic geology students, and Drs. Richard Mauger and Richard Spruill, who afforded me my most memorable and influential teaching experiences, at the UNC System-Wide Geology Field Course.

I am immensely grateful for the people who kept me sane in the swamplands: Charley A. White III, Erin A. (Crawley) and Jackie Stewart. Finally and most importantly, I thank my mother, Myra, and brother, Zeb, for their support and encouragement.

This thesis is dedicated to my father, William Ernest Fuller, for his imitable example as a great teacher both in and out of the classroom; and to my uncles, Bruce Brocksmith Fuller, who lived the life of a scientist despite his training, and Wilson Massey Barnes, Jr., who made his living doing what he enjoyed the most – sailing. The world is lesser for the loss of them, and we miss them terribly.

TABLE OF CONTENTS

LIST OF FIGURES

LIST OF TABLES

INTRODUCTION

The importance of phosphate as an agricultural and industrial mineral resource has stimulated research into deposits in eastern North Carolina and the adjacent continental shelf (Fig. 1). Brown (1958) first described the Miocene phosphorite sediments underlying Beaufort County; significant concentrations of phosphate were later described in the shallow sub-bottom of Onslow Bay (e.g., Miller, 1982; Gibson, 1983; Riggs et al., 1985). The largest concentrations, however, occur in the Miocene primary (formed in-place) phosphorites of the Pungo River Formation and as reworked Miocene phosphate grains in the thin, discontinuous Quaternary surface sediments of the Frying Pan phosphate district of southern Onslow Bay (Riggs et al., 1985; Riggs et al., 1999).

The Quaternary sands in southern Onslow Bay contain a rich assemblage of benthic foraminifera, which are predominantly calcareous. The tests of most calcareous foraminifera are nearly pure (> 99%) $CaCO_3$ in a simple lattice structure (Boyle, 1988); most calcareous foraminifera are calcite, but some taxa secrete aragonite (Loeblich and Tappan, 1988). Among calcareous foraminifera, members of the Suborder Miliolina are unique in having high magnesium calcite (> 4% Mg) and a wall structure composed of a basic layer of calcite laths in random array with inner and outer veneers of tabular crystals that produce a porcelaneous surface texture (Loeblich and Tappan, 1988; Culver, 1993; Boersma, 1978; Haynes, 1981).

Chemical changes that occur during diagenesis (post-deposition) can alter the original composition of foraminiferal tests. Populations of Quaternary benthic foraminifera, in

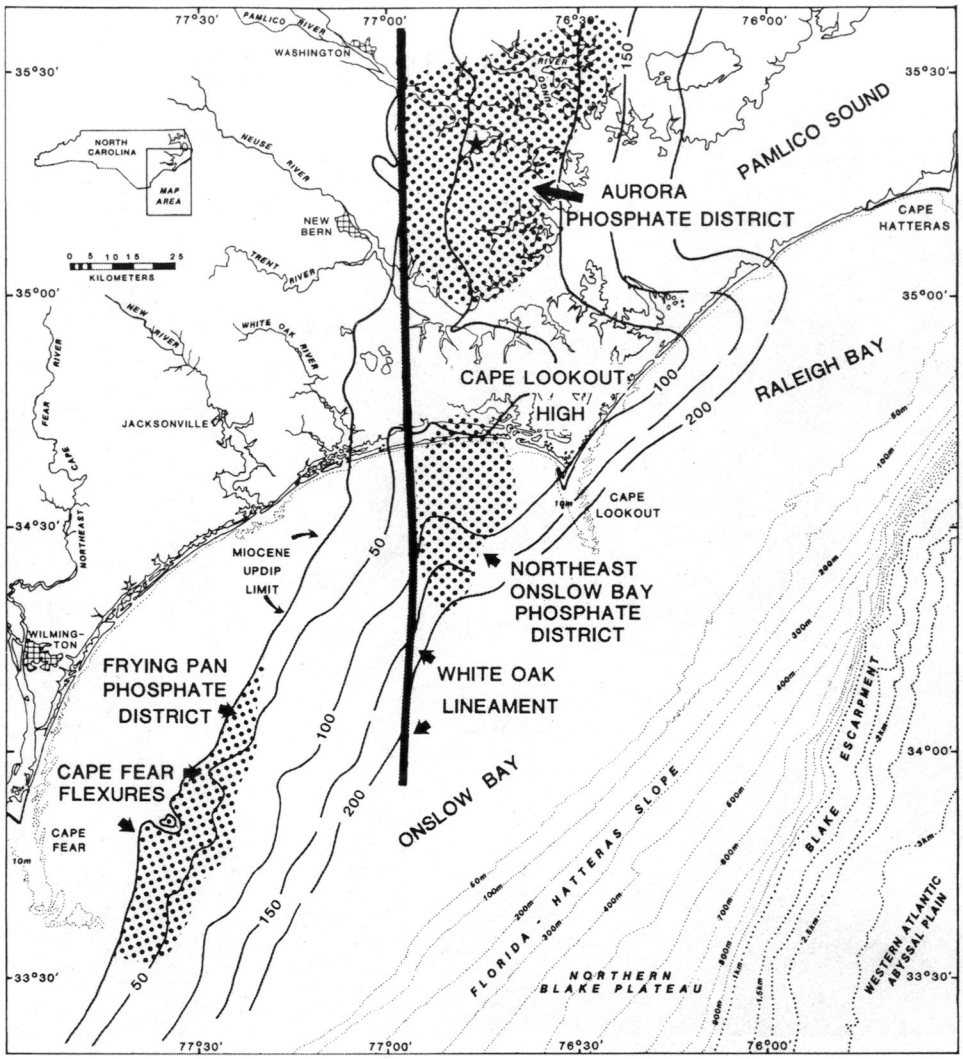

Figure 1. Map of eastern North Carolina coast and continental shelf, showing three major phosphate districts. Solid contour lines indicate thickness of Miocene in meters (from Ellington, 1984).

particular members of the Family Miliolidae and specifically the Genus Quinqueloculina, from the Quaternary sediments of the Frying Pan phosphate district show varying degrees of diagenetic alteration (largely ferruginization). The intensity of ferruginization in the miliolids appears to correlate in areal distribution with the phosphatic character of the underlying Miocene and contiguous Quaternary sediments (Riggs et al., 1985).

STUDY AREA

The Miocene Pungo River Formation is a series of east-southeast dipping, interbedded sands, silts and clays, limestones and dolomites that accumulated in two basins along the North Carolina continental margin (Fig. 1) (Snyder et al.,1988). The emergent Aurora embayment is actively mined for phosphate (Aurora phosphate district), and significant phosphate deposits have also been documented in the Pungo River Formation and Quaternary sands of the Onslow embayment (Northern Onslow and Frying Pan phosphate districts) (Riggs et al., 1985). The Frying Pan phosphate district encompasses the study area for this thesis.

Seismic evidence reveals numerous unconformity-bound, fourth-order depositional sequences within the Pungo River Formation in Onslow Bay that can be grouped into three larger-scale sections (Fig. 2): the middle to late Burdigalian age Frying Pan Section (FPS), Langhian age Onslow Bay Section (OBS), and Serravallian age Bogue Banks Section (BBS) (Snyder et al., 1988). These fourth-order sequences are generally composed of interbedded siliciclastics and carbonates with phosphate content ranging from 2 to 75% (Fig. 3) (Riggs et al., 1985). The seismic sequence terminology will be used in this study to indicate sample provenance, and to facilitate comparisons to published geochemical data.

The southern portion of the Frying Pan Section, known as the Frying Pan phosphate district, is characterized by phosphorite sand (FPS-1) and slightly phosphatic siliciclastic mud lithofacies (FPS-2 and -3), truncated by younger foraminiferal quartz sand and

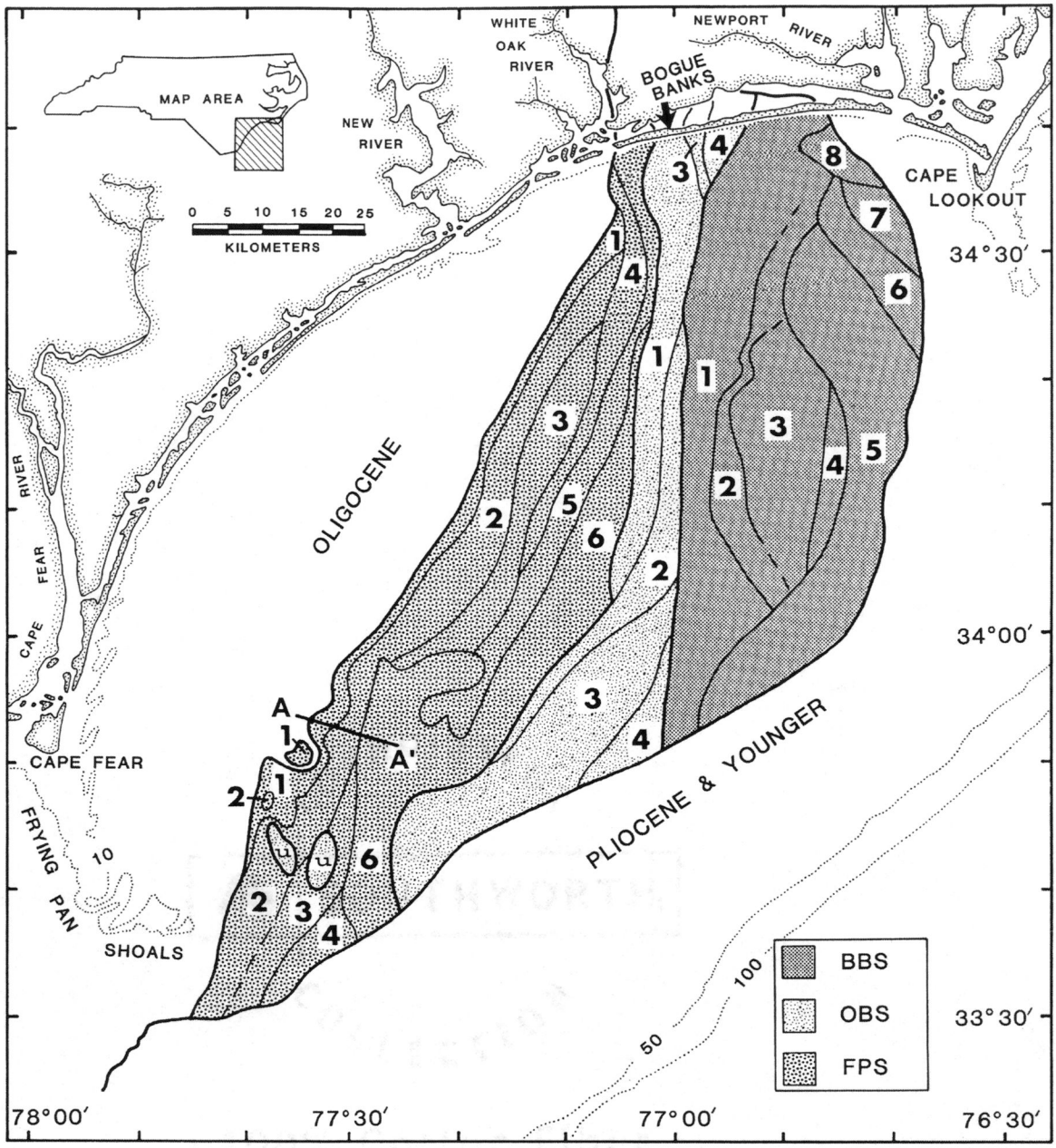

Figure 2. Three Miocene third-order seismic sections – Bogue Banks Section (BBS), Onslow Bay Section (OBS), and Frying Pan Section (FPS) – and their fourth-order subdivisions; u = undifferentiated to fourth-order, erosional outliers in study area (modified from Snyder et al., 1988). Dotted contour lines are depth to seafloor in meters; A-A' line is EN-8C seismic profile shown in Figure 5.

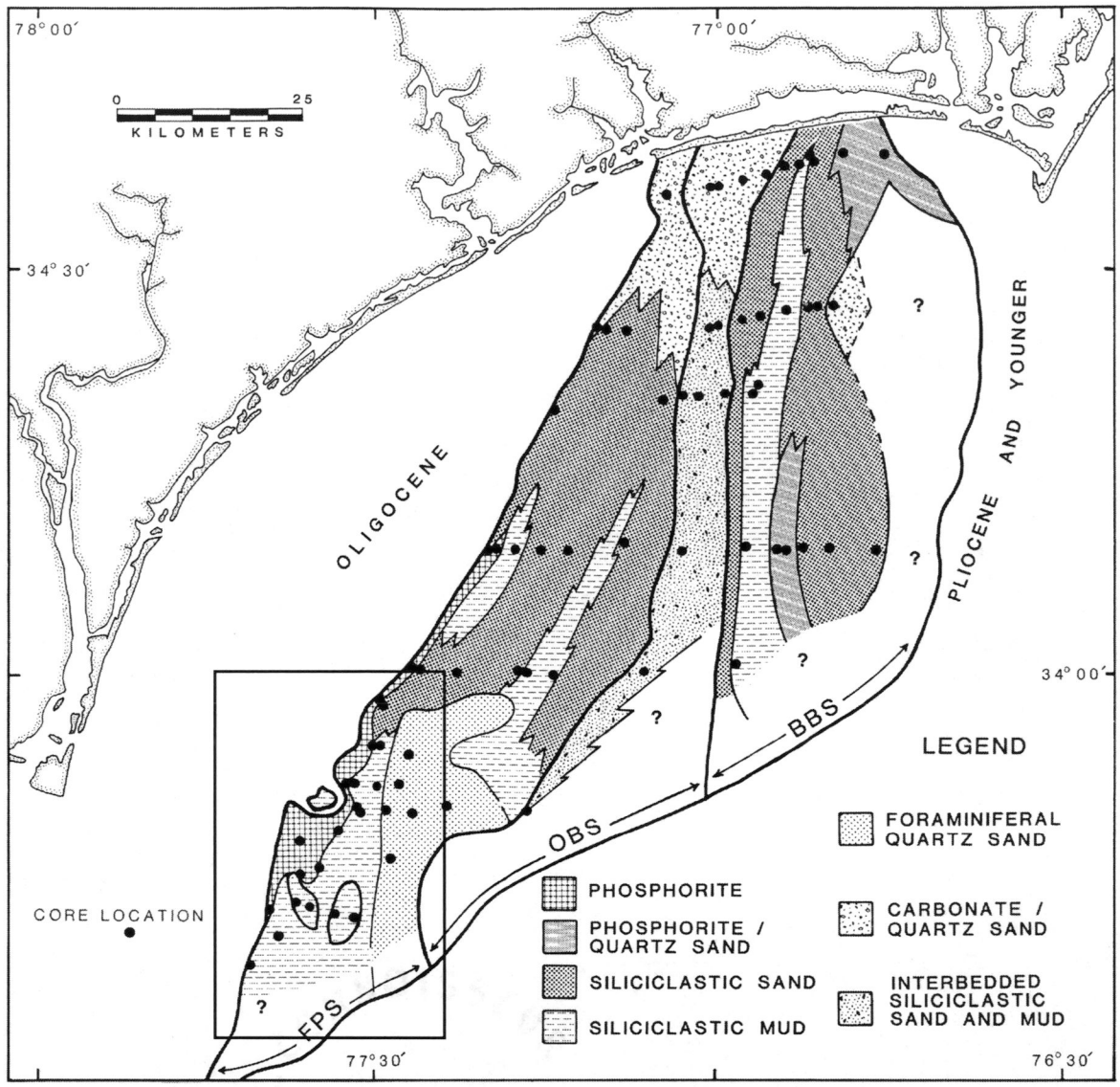

Figure 3. Generalized Miocene lithofacies distribution map superimposed on third-order seismic sequence map (from Snyder et al., 1988). Boxed area is magnified in Figure 6.

fluvial paleo-channel fill (FPS-6) (Figs. 2 and 3) (Snyder et al., 1988). Two units in this district, the fourth-order sequence FPS-1 and the Quaternary sand unit referred to as FPH, contain significant concentrations of phosphate (Riggs et al., 1985).

PREVIOUS WORK

Five National Science Foundation-funded cruises directed by Stanley R. Riggs (R/V *Eastward*, May-June 1980; R/V *Endeavor*, October 1980; R/V *Columbus Iselin*, May 1981; and R/V *Cape Hatteras*, May-June 1982 and May 1983) on the Onslow Bay continental shelf recovered 144 vibracores from the Onslow Bay continental shelf, 95 of which penetrated the Miocene Pungo River Formation (Fig. 4). These cores have been used in a variety of biostratigraphic, lithostratigraphic and geochemical studies, undertaken largely to study the sizeable phosphate deposits in the Miocene Pungo River Formation.

Riggs et al. (1985) concluded that the most economically significant concentrations of phosphate exist in the Frying Pan area (Frying Pan phosphate district) of southern Onslow Bay. Visual inspection of foraminifera collected from the thin, mobile and discontinuous Quaternary sands in this area revealed test discoloration that is unique to the phosphate district. This discoloration, related to diagenetic alteration of the test, appears to intensify with higher phosphate content in the surrounding and underlying sand fractions (Riggs et al., 1984).

Geochemical and Stratigraphic Setting

Generally, phosphate grains are carbonate fluorapatite, a mineral of variable composition resulting from elemental substitutions, admixed with other minerals, including quartz, clay minerals, pyrite and organic matter. Elements associated with these mineral phases include Si (quartz); As, Cd, Cr, Cu, Ni, and Zn (organic matter and

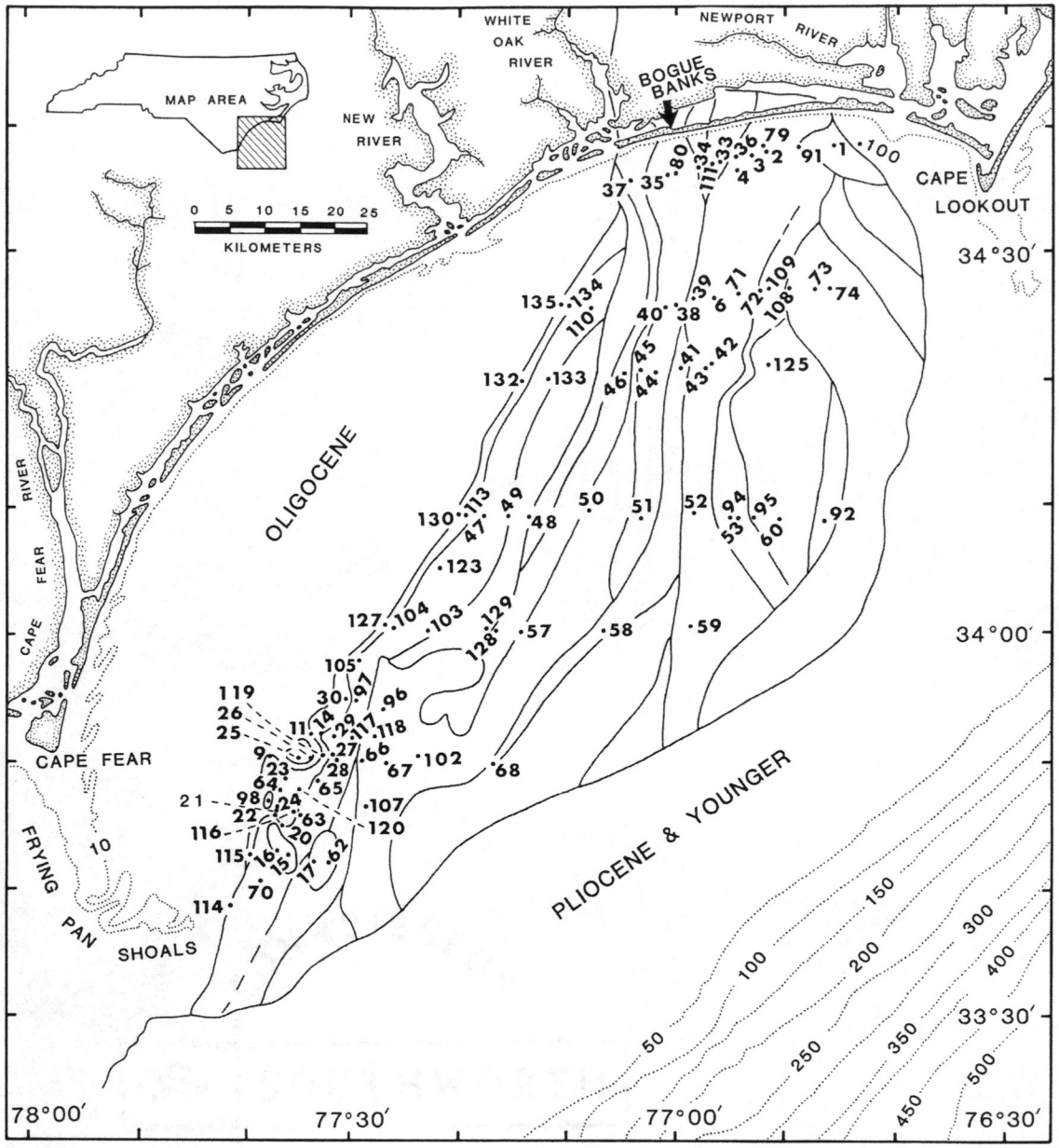

Figure 4. Location of ninety-five vibracores that penetrated the Miocene Pungo River Formation during NSF-funded cruises directed by Stanley R. Riggs (from Snyder et al., 1988). Dotted contour lines are depth to seafloor in meters.

sulfides); Ni (glauconite and iron oxide); As and Mo (pyrite and iron hydroxides); and Fe (iron sulfide, oxide and/or hydroxide). Phosphate grains occur in a variety of morphologies (e.g., pellets, oolites, concretions), each of which can have a unique chemical composition (Ellington, 1984).

In the study area, phosphate grains occur in four morphologies (pellets, intraclasts, microsphorite [see Riggs, 1984, for definition] and skeletal grains) that are distinguishable by chemical composition (Ellington, 1984). Pellets, the most common morphology, are often smooth, fine-grained spheroids with a variety of minor (<5%) inclusions (e.g., pyrite, clay, quartz, organic matter, etc.) in a matrix of microcrystalline carbonate fluorapatite. The coarser, angular intraclasts often contain larger percentages (5-10%) of inclusions, predominantly quartz. Skeletal grains are primarily carbonate fluorapatite with few included materials, and microsphorites contain the highest percentage of inclusions.

The seismic unit FPS-1 thickens and dips eastward under units FPS-2, -3 and -6, and is deeply incised by channel-fill sediments from unit FPS-6 along the eastern boundary of Burdigalian sediments (Fig. 5). The phosphate in FPS-1 is predominantly pelletal, smooth, and dark brown or black in color, with an average P_2O_5 concentrate grade of 29.2% (Riggs et al., 1985). Through spectroscopy and factor analysis, Ellington (1984) determined that the phosphate component in FPS-1 is principally carbonate fluorapatite; small amounts of included clay minerals, iron sulfides, iron oxides and organic matter control the concentration of major (Al, Fe, Si, K, Ti) and trace (As, Cr, Mo, Ni, V) elements (Ellington, 1984).

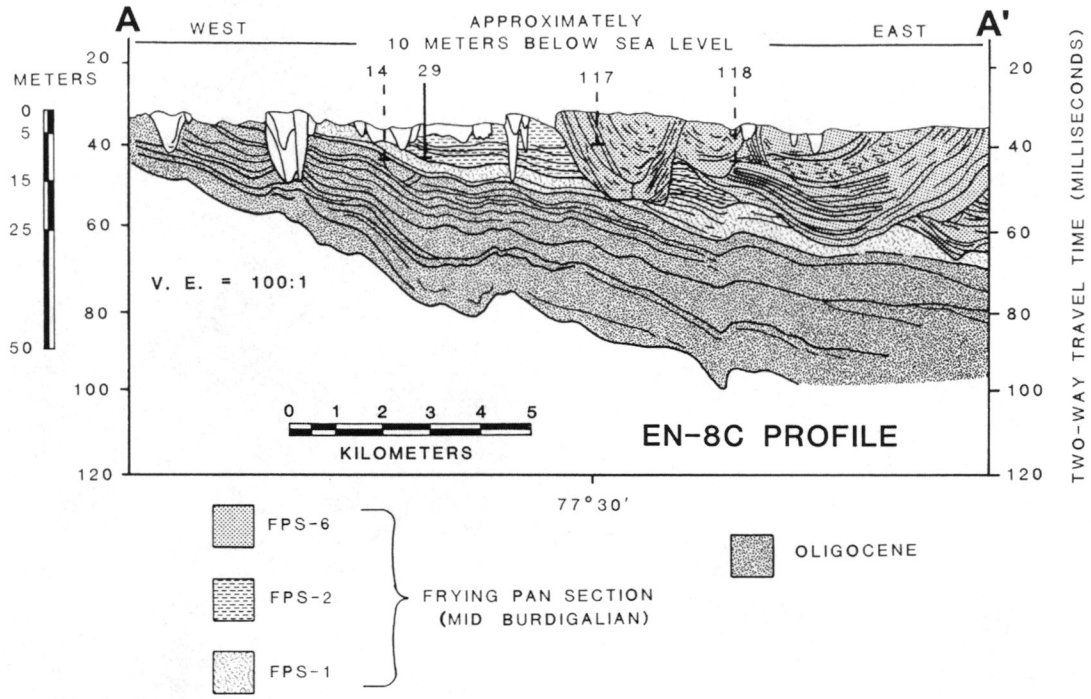

Figure 5. The west-east EN-8C seismic profile across Frying Pan phosphate district, shown as A-A′ on Figure 2 (vertical exaggeration 100:1) (modified from Snyder et al., 1988).

The thin (0-1.5 m), discontinuous FPH sand sheet overlying the FPS units contains mostly pelletal phosphate that is pitted and dull, light brown to ocher, with an average P_2O_5 content of 6.3% (Riggs et al., 1985). Figure 6 delineates the extent of significant phosphate deposits in FPH as a plot of the 3% P_2O_5 contour. Spectroscopic analyses of FPH phosphate pellets show high Fe and As, and low Cd, Zn and Mo values. These enrichments and concomitant depletions suggest oxidation of organic materials, and possibly iron sulfides, producing precipitates of iron oxide and/or hydroxide (Ellington, 1984).

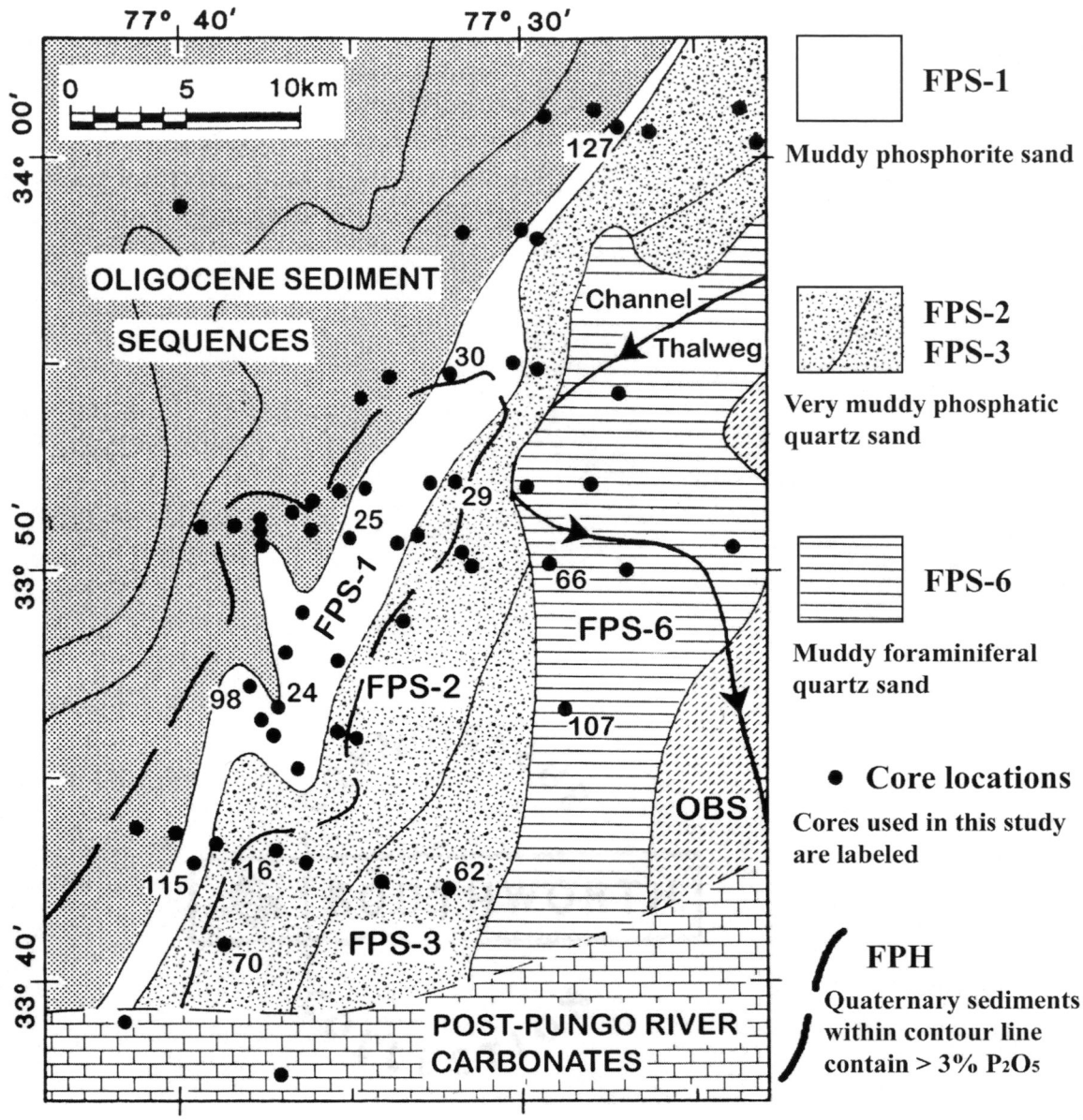

Figure 6. Map of areal extent of significant concentrations of phosphorite (> 3% P_2O_5) in Quaternary sediments (FPH); on map of seismic units in the Frying Pan phosphate district (modified from Riggs et al., 1985). Boundaries with the Miocene Onslow Bay Section (OBS), Oligocene sediments and post-Pungo River carbonates are shown. Location of map shown on Figure 3.

Paleontological Work

Visual inspection of foraminifera from the Quaternary sands of the Frying Pan phosphate district revealed surface discolorations that progress from late- to early-formed chambers and correlate with phosphate content in the sand fraction of the sample. Several specimens of the miliolid foraminifer *Quinqueloculina lamarckiana* d'Orbigny were analyzed by microprobe to determine the composition of the tests in various stages of replacement (Riggs et al., 1984). The analysis revealed the alteration is primarily ferruginization, with minor phosphatization, that decreases from exterior (mean value of 7-18% FeO, 0.4-0.8% P_2O_5) to interior (mean value of 6% FeO, 0.3% P_2O_5) chamber walls (Fig. 7). Chamber fill is predominantly ferruginous and black in color. The spatial distribution of altered tests generally coincides with the concentration of phosphate in the underlying Miocene sediments and the surrounding Quaternary sands (Riggs et al., 1984).

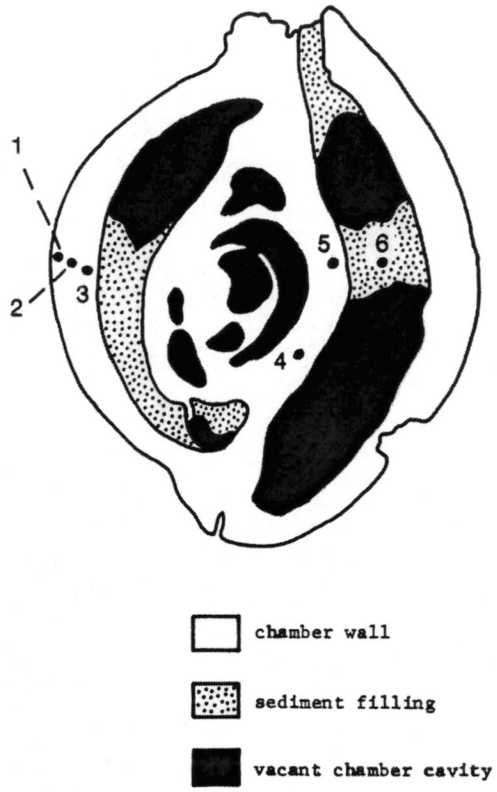

Analysis	Exterior Chamber Wall			Interior Chamber Wall		Chamber Fill
	Outside	Middle	Inside	Adj. Full	Adj. Empty	
**	1	2	3	4	5	6
% MgO	4.6	4.5	4.6	3.9	4.7	7.8
% FeO	10.9	5.9	4.4	1.6	2.5	35
% CaO	41	46.4	49.4	53.1	51.7	0.8
% P_2O_5	0.5	0.3	0.2	---	0.2	1.2
% Al_2O_3	0.6	0.3	0.1	---	---	5.2
% SiO_2	1.2	0.4	0.4	---	0.2	17.5
% K_2O	---	---	---	---	---	0.2
% SO_3	0.6	0.6	0.8	0.8	0.6	0.2
TOTALS	55-63%	56-60%	60%	60%	60%	53-85%
n =	6	5	2	1	1	6

Figure 7. Microprobe analysis of foraminifera from the Quaternary sands of the Frying Pan phosphate district. ** = point location numbers shown in sketch of test above (modified from Riggs, Snyder, Spruill and Mauger, unpublished figure).

PURPOSE OF STUDY

A relationship between the alteration of foraminiferal tests and the spatial distribution of phosphorites in the Frying Pan phosphate district was indicated by the microprobe work performed on a limited number of specimens (Riggs et al., 1984). In order to investigate this relationship on a regional scale, rapid multi-elemental analyses of large numbers of diagenetically altered miliolids from the surficial sediments of twelve core locations in the phosphate district were performed using proton induced x-ray emission (PIXE) spectrometry.

Analysis of whole populations in various stages of alteration can provide chemical signatures for each sample that can be compared with existing geochemical data for the underlying and surrounding sediments. The elemental signature of the foraminiferal samples serves as a basis to investigate the relationship of the areal distribution of phosphorites in the underlying Miocene and surrounding Quaternary sediments with diagenetic alteration in foraminifera. Specifically, this study seeks to:

1. Test whether ferruginization, currently documented by microprobe analyses on only a few specimens, is in fact the dominant type of alteration throughout the Quaternary sands of the Frying Pan phosphate district;
2. Test whether visual estimates of the extent of alteration among foraminifera accurately reflect the extent and spatial pattern of alteration as determined analytically by PIXE;

3. Provide semi-quantitative estimates of the scale of alteration across the area; simple specimens counts can be misleading in that numerous small specimens may contain a greater amount of iron product than fewer but larger specimens;
4. Test the hypothesis that the aerial distribution and concentration of iron product is related to the distribution of underlying Miocene phosphorites and reworked phosphate grains that co-occur with foraminifera in the Quaternary sands;
5. Make inferences about the source of iron product in foraminifera of the Quaternary sands of southern Onslow Bay using selected miliolids as a proxy for the entire foraminiferal assemblage.

PROCEDURES

Sample Selection

The 144 vibracores recovered during the five previously mentioned National Science Foundation-funded cruises in Onslow Bay were taken with a compressed-air driven vibracoring rig with a maximum penetration depth of 9 m (Mallette, 1986). The twelve cores included in this study (Fig. 8) were selected because: 1) they penetrate the thin, discontinuous Quaternary surface sediments in southern Onslow Bay; 2) they provide east-west and north-south transects over areas of highest phosphate concentration in the Pungo River Formation; and 3) they contain sufficient numbers of miliolids to analyze using the methods described below (see *Analysis*).

Quaternary sediments in southern Onslow Bay, unlike the Pungo River sediments, contain little silt or clay, and therefore require minimal processing in order to recover foraminifera. Each sample, comprised of sediment from the uppermost 50 cm of the vibracores, was soaked in a weak Calgon solution for approximately 24 hours, then boiled for about one-half hour in a weak solution of Quaternary "O" (alkyl imidazolinium chloride) to deflocculate clays. The samples were washed over 1.41 mm and 63 μm mesh screens to remove clays and concentrate the foraminifera (Moretz, 1988). This fraction was further reduced by microsplitting to a practical size for this study.

Specimens of two species, *Quinqueloculina lamarckiana* d'Orbigny and *Q. bicarinata* d'Orbigny, were selected for PIXE analysis. These two species are commonly occurring, susceptible to alteration, and large enough to provide sufficient sample for

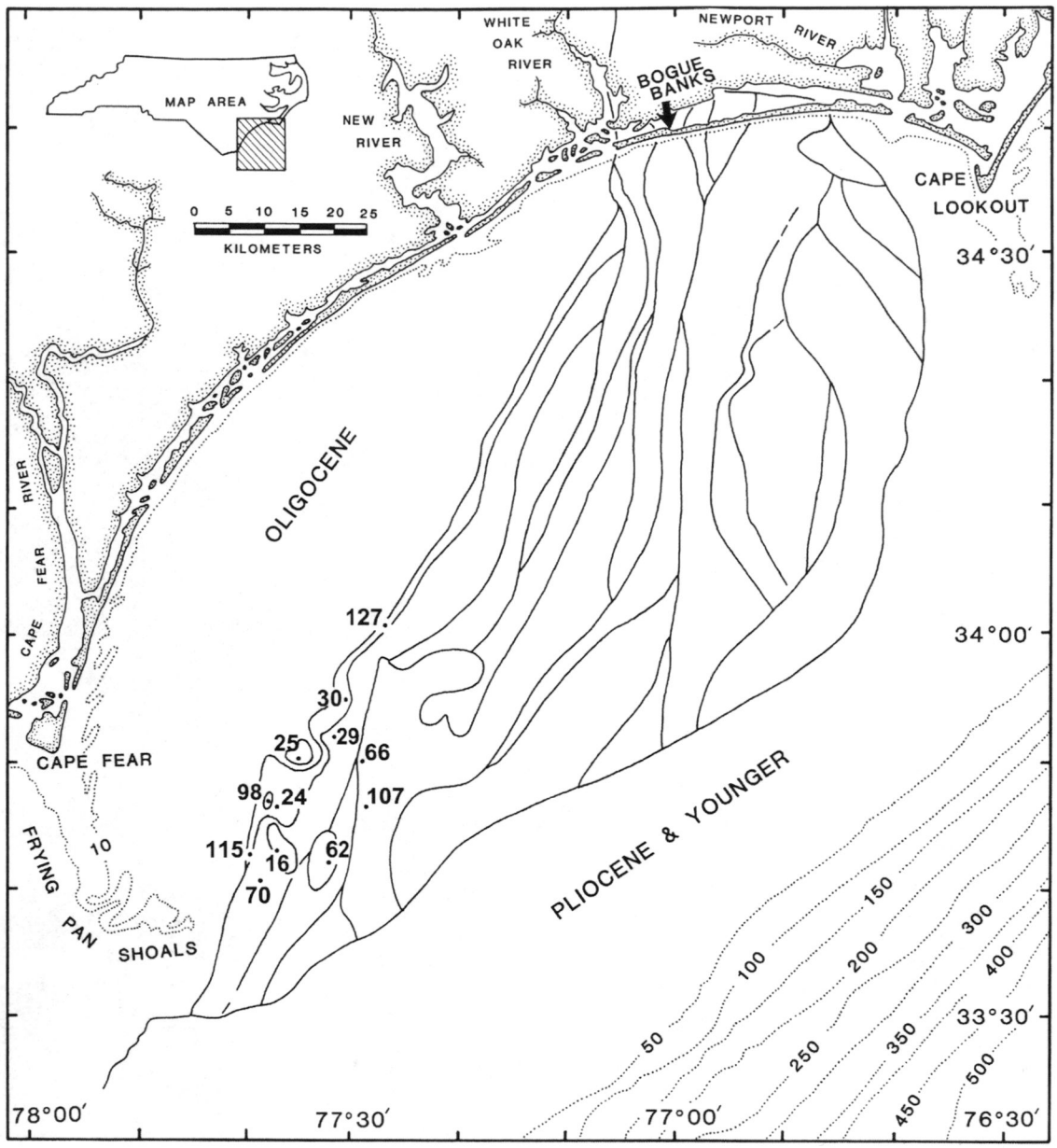

Figure 8. Location of the twelve vibracores used in this study, selected from core locations shown in Figure 4 (modified from Snyder et al., 1988).

analysis. Whole and nearly whole specimens of *Q. lamarckiana* and *Q. bicarinata* in all stages of alteration were picked from each sample under a binocular microscope using a fine, moist sable-hair brush. All specimens from the microsplitter aliquot were picked to ensure that the samples were representative and unbiased. Picked specimens were then separated into three categories, based on visual assessment of the degree of alteration: 1) unaltered (less than 10% altered); 2) partially altered; 3) altered (more than 90% altered) (Fig. 9).

Final test counts varied greatly between samples, from 16 to 512 tests per sample, and test size ranged widely within and between samples (Table 1). In order to prevent bias, all specimens were counted and used in the final analysis. This allowed for the greatest sample weight and volume from all twelve samples, but hindered direct comparison between samples (a problem circumvented by using Ca:Fe ratios, as explained below). To measure sample masses reliably, the microbalance was calibrated each morning and again after every 20 uses with a one-gram standard. All weights were taken within one week and at each measurement the microbalance was allowed to stabilize (up to 10 minutes).

For each sample, specimens were separated into the three visually assessed alteration categories – altered, partially altered, and unaltered (Fig. 9) – and the tests in each category were counted and weighed in aluminum weight boats. After these numbers were recorded, all of the tests were recombined into a single weigh boat and weighed as a group (Table 1). These combined groups of specimens were then subjected to the cleaning process described below (see *Cleaning Method*).

Figure 9. Idealized alteration sequence of miliolids from Quaternary sediments, with category labels (modified from Riggs et al., unpublished figure).

In addition to the twelve combined samples, three control samples (designated by a small "c" following the core number in tables and text) were prepared in the manner described above (Table 1). The aliquot picked and analyzed for OB-127c is an order of magnitude larger than the aliquot produced for the combined sample OB-127. The three alteration categories in these control samples were weighed, cleaned and analyzed separately to verify the relationship between increasing iron content and visual alteration in the sample set.

Cleaning Method

The concentration of trace metals can be significantly affected by sediment trapped in the hollow chambers of the test (Boyle, 1995). In this study, preliminary PIXE analyses of foraminifera processed through various cleaning techniques revealed significant reduction in trace element concentrations after cleaning. Boyle (1981, 1995) evaluated various cleaning methods to determine the best system for removing contaminants; his recommended methodology, used in this study, removes contaminants from the chambers

	SAMPLE	Alteration Category	Specimen Count	Weight (mg)	Combined Count	Combined wt. (mg)	Final sample volume (μL)
combined samples	OB-16	unaltered	195	2.66	296	5.15	2709
		part. alt.	66	1.49			
		altered	35	1.47			
	OB-107	unaltered	66	1.24	128	2.27	1564
		part. alt.	49	0.86			
		altered	13	0.44			
	OB-30	unaltered	25	0.72	36	0.76	882
		part. alt.	11	0.26			
		altered	0	0.00			
	OB-24	unaltered	23	1.12	57	3.57	2074
		part. alt.	14	0.92			
		altered	20	1.79			
	OB-66	unaltered	5	0.14	16	0.76	772
		part. alt.	5	0.15			
		altered	6	0.60			
	OB-62	unaltered	16	0.48	148	3.55	1986
		part. alt.	79	1.61			
		altered	53	1.78			
	OB-127	unaltered	35	1.00	47	1.15	948
		part. alt.	12	0.27			
		altered	0	0.00			
	OB-70	unaltered	36	1.62	267	16.85	4007
		part. alt.	72	3.61			
		altered	159	12.12			
	OB-25	unaltered	138	3.11	223	6.94	3039
		part. alt.	64	2.76			
		altered	21	1.47			
	OB-115	unaltered	12	0.04	41	1.90	1123
		part. alt.	8	0.36			
		altered	21	1.47			
	OB-29	unaltered	13	0.41	19	0.90	1024
		part. alt.	1	0.12			
		altered	5	0.42			
	OB-98	unaltered	33	1.48	104	6.31	3007
		part. alt.	38	2.21			
		altered	33	2.75			
control samples	OB-70c	unaltered	67	3.94	258	15.39	1178
		part. alt.	150	10.31			2103
		altered	41	1.14			2281
	OB-24c	unaltered	36	2.13	85	4.18	914
		part. alt.	24	1.17			1264
		altered	25	0.88			1002
	OB-127c	unaltered	79	0.73	512	6.67	3392
		part. alt.	20	0.48			750
		altered	413	5.46			640

Table 1. Sample preparation statistics – cores listed in order of PIXE analysis. Control samples were not combined; calculations of combined count and mass (in gray) are presented for comparison. Combined weight includes loss during the recombination and reweighing process; final sample volume is the result of the cleaning process (see text).

and from surface films on the test (Appendix A). To prevent cross-contamination, micropipette tips were replaced for each sample treatment, samples remained tightly capped when stored or in the ultrasonicator or centrifuge, and all tools were cleaned and rinsed repeatedly with deionized water.

Each individual specimen was crushed gently with a glass plate to open up the chambers, and the fragments were swept into a micro-centrifuge tube labeled with the core number (and alteration category, in the case of the control samples). Clay-size particles were removed by ultrasonic cleaning and repeated rinsing with deionized water and glass-distilled methanol. The samples were rinsed in an ultrasonic bath with a reducing reagent of anhydrous hydrazine, ammonium hydroxide and citric acid to remove metal oxides. To remove organic matter, the samples were heated to about 80°C in an oxidizing solution of H_2O_2 and 0.1N NaOH, and periodically ultrasonicated. The samples were then rinsed with a weak acid leach of 0.001N HNO_3. Finally, the samples were dissolved (pH<4) in 0.075N HNO_3 in the ultrasonic bath (to speed dissolution) and centrifuged for 5 minutes.

Under a laminar flow hood, using a micropipette calibrated to 5.5 µl, the supernatant was siphoned off each sample and dropped onto the center of a thin aluminized film covering a 3 cm diameter polyvinyl chloride (PVC) ring. Each 5.5 µl drop was allowed to dry before another drop was applied, constraining the final sample area to approximately 5 mm^2. The air-drying process may have produced variations in thickness of sample across the 5 mm^2 area. The sample rings were stored in lidded plastic vials,

which were designed to keep the sample surface suspended, to prevent contamination during transportation and storage.

Analysis

Elemental analyses were performed using proton induced x-ray emission (PIXE) spectrometry, a non-destructive method of multi-elemental analysis used in a variety of research disciplines. PIXE uses charged particles to irradiate a sample, exciting atoms in the sample that can then emit characteristic x-rays. Depending on the design of the system, PIXE can analyze for elements with atomic number around 13 and greater to the parts per million range (ppm) (Johansson, et al., 1995). An energy dispersive x-ray detector collects the x-rays and produces a histogram, or spectrum, of x-ray counts of each element.

The PIXE spectra are analyzed using GUPIX, an analysis program produced by the Guelph Scanning Proton Microprobe (GSPM) Laboratory at the University of Guelph in Guelph, Ontario, Canada. Given various detector and sample parameters, GUPIX calculates the peak intensities of the spectra using a modified least squares procedure, and converts the peak area into element concentration. The software presents the concentrations, limits of detection (LOD), statistical and fit error estimates, and spectrum plots.

Proton Induced X-ray Emission (PIXE) Spectrometry

PVC rings loaded with sample are placed in a revolving sample wheel inside the PIXE vacuum chamber of the accelerator (Fig. 10). A sputter ion source produces negative ions and electrons. The negative hydrogen ions (H^-) are accelerated to 60 keV in an evacuated beam line, magnetically separated from other negative ions and injected into the accelerator, where they are further accelerated to the positive potential of the electrostatic accelerator. At the high voltage positive terminal of the accelerator, the electrons are stripped from the H^- ions, producing protons that are further accelerated to ground potential. After exiting the accelerator, the charged particles pass through an analyzing magnet that further isolates the protons from heavier ions.

A 1 mm graphite collimator produces a uniform beam of protons that bombards each sample in the vacuum chamber, causing inner shell electrons to be ejected from the atoms in the sample (Coulomb interaction) (Fig. 11). The de-excitation of the atom typically produces a characteristic x-ray for each element as an electron from an outer shell fills the inner-shell vacancy (surplus energy may also be dispersed by an Auger electron). The x-ray energy is equal to the difference in the binding energy of the outer and inner shells. Each sample was positioned so that the beam bombarded the approximated center of each sample drop, reducing background contribution to the analysis.

The x-rays are collected by a lithium drifted silicon [Si(Li)] detector that produces a histogram of characteristic K_α, and sometimes K_β, x-ray lines for each element in the specimen. Si(Li) detectors can be overwhelmed by high count rates that simultaneously

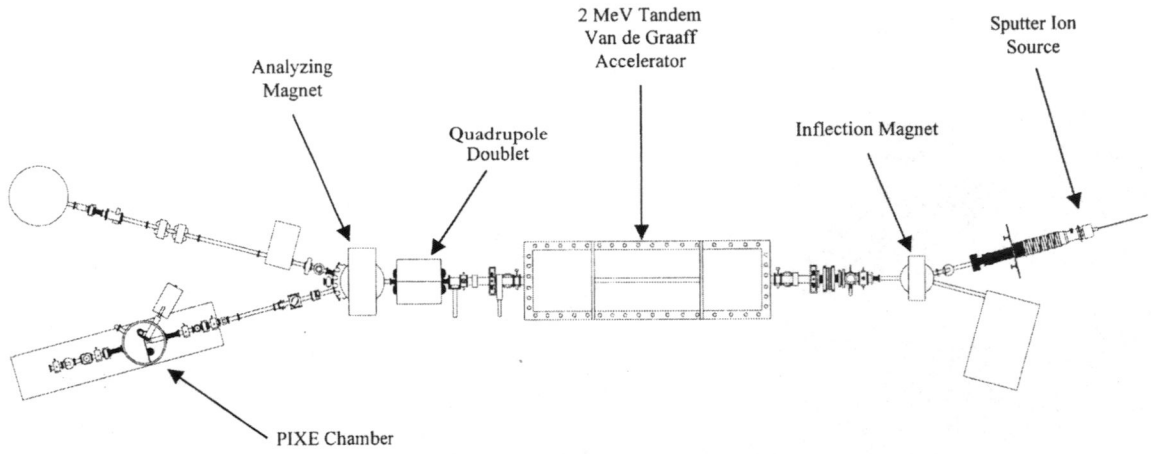

Figure 10. Schematic of the East Carolina University 2 MV tandem Van de Graaff accelerator and its components (modified from Fogle, 2000).

present multiple x-rays at the detector window. At high count rates, the individual x-rays may be processed as one single peak with energy equal to the sum of the individual x-ray energies (pile-up) (Johansson et al., 1995). In order to prevent pile-up x-rays from calcium (Ca), a light element with a large probability for excitation and the major component in the study samples, beam intensity and count rate are kept low. However, this approach slows the accumulation of heavier element x-rays significantly, because of the low probability for K-ionization of the more tightly bound inner-shell electrons. To detect heavier elements, the samples were re-analyzed under higher ion intensity, using a filter to preferentially absorb the lower-energy Ca x-rays.

Variations in the beam intensity and count rate were constrained as much as possible between sample analyses by monitoring and adjusting the energy and focus of the proton beam. Count rates were improved and pile-up reduced through micro-positioning of the sample. Environmental conditions during some analyses hindered accurate readings of

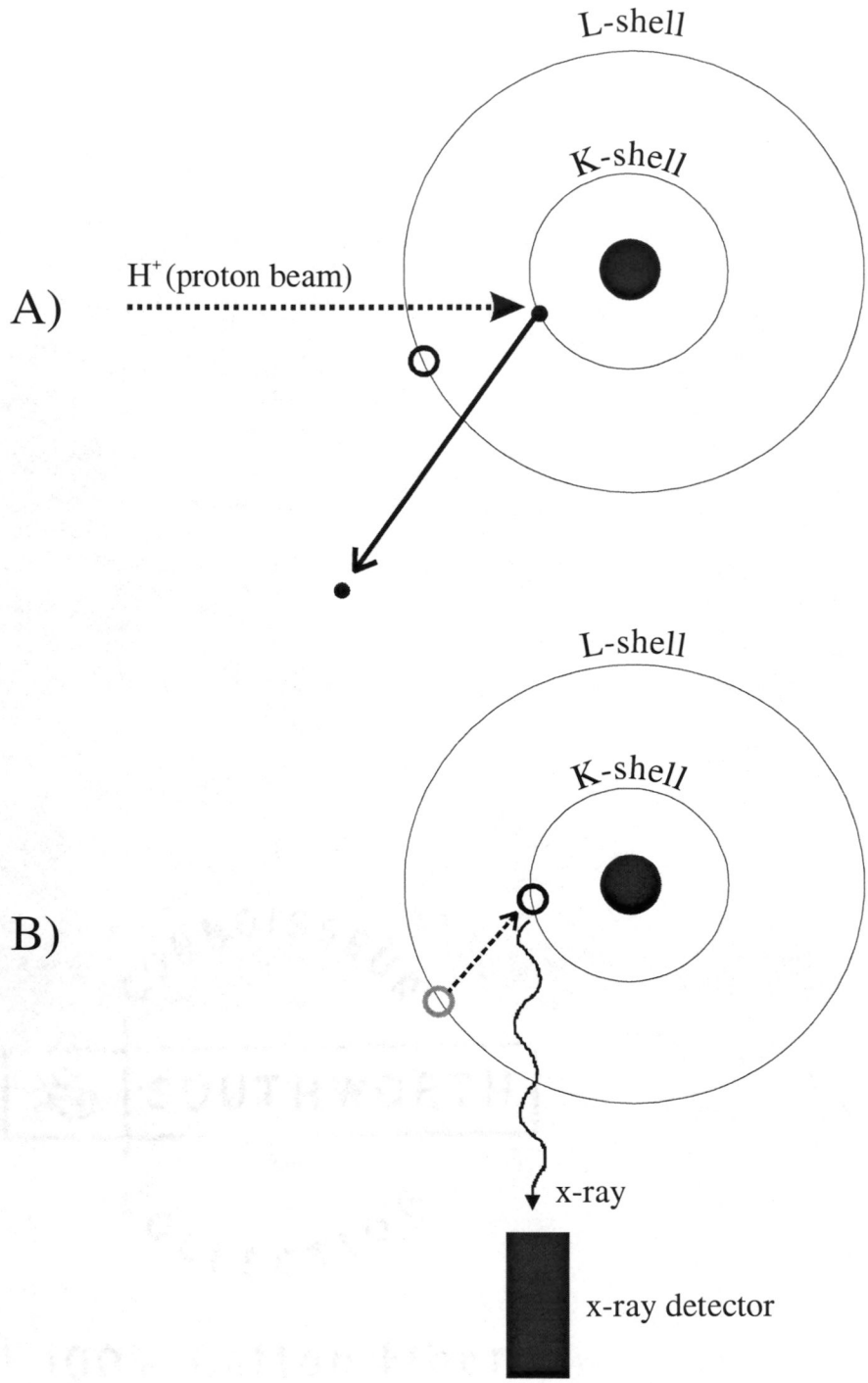

Figure 11. Simplified sketch of Coulomb interaction, showing: A) proton beam bombarding a K-shell electron (black dot), which is then ejected; and B) the atom then de-excites by transitioning an L-shell electron (hollow circle) into the K-shell vacancy; the excess energy is emitted as a detectable x-ray (modified from Fogle, 2000).

samples; subsequent analyses provided more reasonable trends. Unmeasured or variable parameters such as sample thickness, beam intensity, run time, and filter thickness, make absolute yields difficult to obtain from GUPIX. For this study, concentration measurements are converted to ratios normalized to calcium to define the chemical signatures of the samples.

GUPIX Analysis

The GUPIX program uses a non-linear least squares fit (Marquardt type) followed by linear least squares fit to obtain relative line intensities from the x-ray spectra. GUPIX converts these peak areas into element concentrations, and presents the data with a variety of fit information (Appendix B; Maxwell et al., 1995). GUPIX is designed for analysis of thin targets, such as the samples in this study, which allow the proton beam energy to pass through the sample effectively unchanged. Given a thin target designation, GUPIX describes x-ray yields for the sample in terms of areal density (x-rays per microCoulomb per ng/cm^2 per steradian), and concentrations are reported in units of ng/cm^2 (Maxwell et al., 1995).

PIXE analyses of the study samples were preceded by analysis of two standards, which are used to calibrate the peak fit process in GUPIX. Spectral peaks for these standards were plotted and fit by linear least squares regression to determine channel offset (intercept) and change in energy per channel (slope). The parameters for these standards were used as the initial settings for subsequent GUPIX analyses; some fit parameters were allowed to drift during iteration to produce the most appropriate peak fit.

During GUPIX analysis, the spectra were frequently checked for accuracy based on the fit of the dominant Ca peak.

Each spectrum was visually inspected prior to GUPIX analysis to determine which elements showed significant peaks. GUPIX allows for the evaluation of up to 60 elements during each spectral analysis, and presents concentration output with fit and detector efficiency information to help the user verify the accuracy of the results. The user can manipulate the fit parameters to improve peak fit, and change fit elements to produce the most accurate reading of relevant elements.

Initially, most spectra were analyzed for Ca, Sc, Mn, Fe, Zn and Sr; some were also analyzed for Co, Cu and Cr. Elements were accepted for final analysis if their reported concentration was significantly higher than the limit of detection (LOD), and fit and statistical error were lower than 15%. GUPIX then reiterates the calculations to produce more accurate readings for those elements.

Analytical Parameters

Initially, all samples were analyzed for 600 seconds (10 minutes), with an average beam intensity of 2.0 nannoamps (na) and average x-ray count rate of 361 counts per second (cps) (Appendix C-a). During these analyses on October 6, 2003, heavy construction outside the laboratory caused major vibrations that affected both the beam and detector, resulting in significant inconsistency between sample analyses. The control samples were also analyzed on this day, although variations in beam strength and count rate made these results unusable (Appendix C-a). The low intensity and count rate during the October 6th (*1006)* analysis inhibit the accumulation of minor and trace elements

beyond their LODs; spectra from *1006* were analyzed by GUPIX for Ca, Fe and Sc (see *Discussion*); one sample was analyzed for Zn (Appendix C-a).

In order to capture significant x-ray counts from heavier trace elements, a 0.05 mm-thick aluminum filter (#2) was placed in front of the detector window. This filter preferentially absorbs lighter x-rays from elements, including Ca, the major element in the sample. On October 13, 2003, the samples were analyzed for 600 secs, with an average beam intensity of 12.0 na and an average x-ray count rate of 295 cps (Appendix C-b). The control samples were also retested under these conditions, yielding more reliable count rates. GUPIX was able to return significant peak areas for Ca, Fe and Zn for most samples. Sr and Mn were present in some samples, although their fit and/or statistical error were relatively high (10-15%) (Appendix C-b)

On November 18, 2003, the samples were subjected to an unfiltered PIXE analysis of 1200 secs, in which count rate and beam intensity were most strictly constrained between samples (averages of 344 cps, 1.45 na) (Appendix C-c). The control samples were not tested during this analysis. The GUPIX output clarifies the results from *1006* analysis and reveals a few trace elements with fit/statistical error over 10% (Appendix C-c).

RESULTS

Although the analyses on October 6 (*1006*), October 13 (*1013*) and November 18 (*1118*), 2003, produced similar Fe:Ca ratios, the *1118* analysis of the combined samples is interpreted to be the most reliable because of the consistency of the beam intensity and count rate throughout the analysis. These parameters were also reliably constrained during the *1013* analysis of the control samples; due to time constraints, the control samples were not analyzed during the *1118* analysis. Hence, the *1118* results are used to compare to previously published geochemical data in order to investigate relationships. The *1013* analysis are used to discuss the control samples and the presence of trace elements. Disparity between the ratios produced by the analyses can be attributed to variance in sample thickness associated with the targeted spot on the sample, total analysis time, and beam intensity changes during and between analyses.

Analyses of Control Samples

A general trend of increasing iron concentration that parallels test alteration can be seen in Figure 12. This is particularly clear in OB-24c, which benefits from having a similar number of tests in all three categories and consistent beam parameters during the three analyses; the 25 altered foraminifera have nearly twice the iron concentration (1.36%) of the 24 partially altered specimens (0.70%) (Table 2). In OB-24c and OB-127c, the larger group of unaltered tests contain nearly six times less iron than the smaller numbers of partially altered tests.

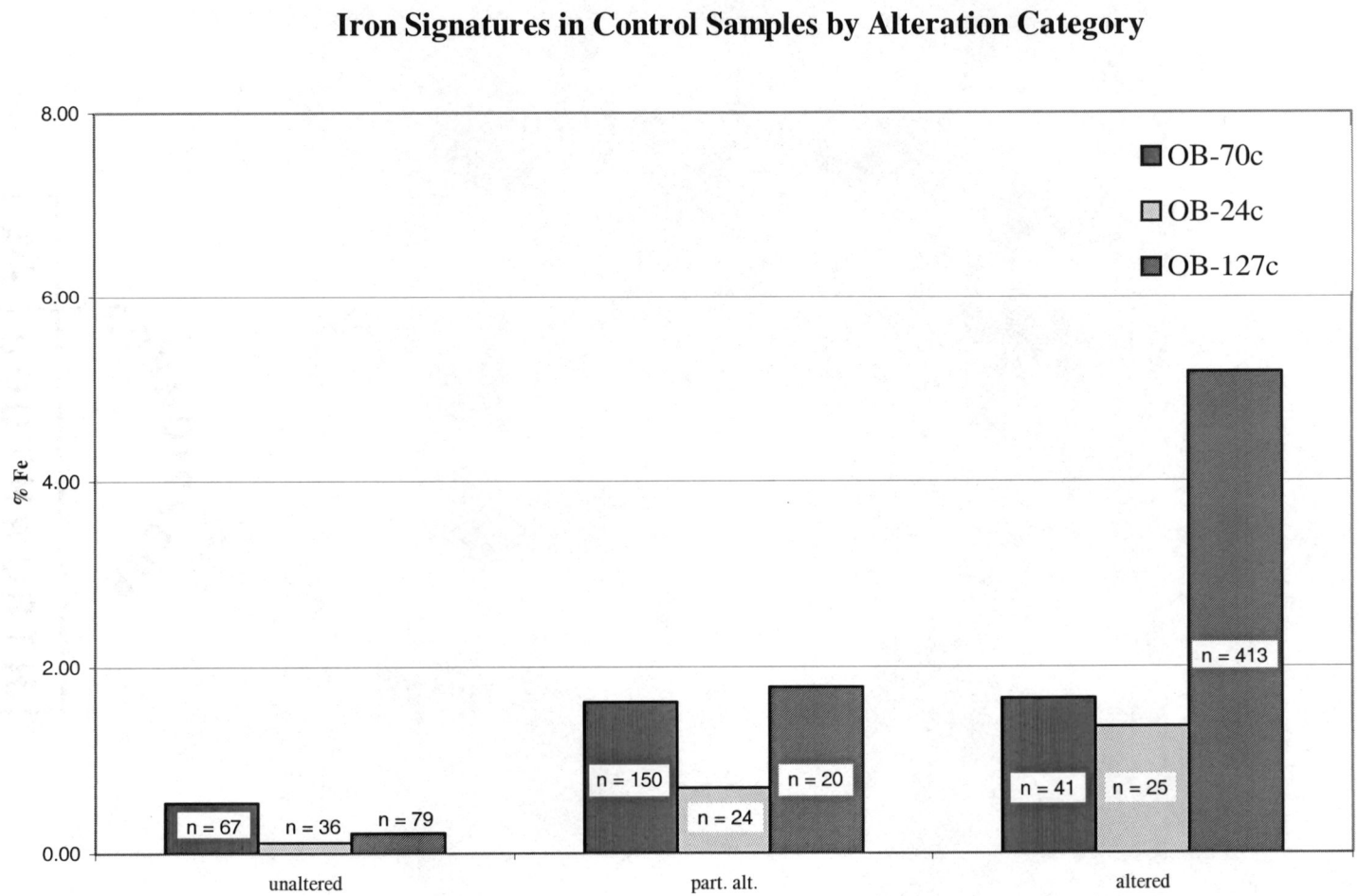

Figure 12. Plot of control sample iron signatures by alteration category, n = test counts.

SAMPLE	Alteration Category	Specimen Count	Weight (mg)	% Alteration by count	% Alteration by mass	1013 Fe/Ca ratio
OB-70c	unaltered	67	3.94	26	26	0.0054
	part. alt.	150	10.31	58	67	0.0162
	altered	41	1.14	16	7	0.0166
OB-24c	unaltered	36	2.13	42	51	0.0012
	part. alt.	24	1.17	28	28	0.0070
	altered	25	0.88	29	21	0.0136
OB-127c	unaltered	79	0.73	15	11	0.0022
	part. alt.	20	0.48	4	7	0.0178
	altered	413	5.46	81	82	0.0518

Table 2. Control sample population statistics and PIXE/GUPIX *1013* analyses results.

In OB-70c, the 150 partially altered foraminifera contribute nearly the same iron concentration as the 41 altered specimens, suggesting originating population size is a contributing factor to iron signatures in the samples. As noted in the microprobe work (Riggs et al., 1984), ferruginization is most intense on the outside of the exterior chamber wall, thus a greater population size (i.e., more surface area) may contribute a higher iron signature than a population with fewer numbers. This can be extended to the study samples by considering the effect of the numbers of tests that constitute the alteration categories. In most samples, mass per individual test increased slightly from unaltered to altered tests.

Analyses of Combined Samples

The largest concentration of iron (approximately 9.8%) occurs in foraminifera from OB-115; the number and weight percentages of altered and partially altered tests dominate the picked specimens in this sample (Table 3, Fig.13). A similar population of foraminifera at OB-62 yields an iron signature of 6.8%. OB-29 contains significant concentrations of iron (approx. 6.6%), although test counts are strongly skewed towards unaltered specimens. The total test count is low in this sample, and size variation among the specimens causes the numerically scarcer but heavier altered and partially altered tests to outweigh the greater number of unaltered tests. OB-16 is mostly populated by unaltered foraminifera, but partially altered and altered specimens again outweigh the unaltered specimens, producing an iron signature of approximately 3.7%. OB-98, at nearly 3.0% Fe, contains similar numbers of specimens in each alteration category. A greater number of unaltered foraminifera, but heavier partially altered and altered

SAMPLE	Alteration Category	Specimen Count	Weight (mg)	% Alteration by count	% Alteration by mass	1118 Fe/Ca ratio	rank
OB-16	unaltered	195	2.66	66	47	0.0365	4
	part. alt.	66	1.49	22	26		
	altered	35	1.47	12	26		
OB-107	unaltered	66	1.24	52	49	0.0168	10
	part. alt.	49	0.86	38	34		
	altered	13	0.44	10	17		
OB-30	unaltered	25	0.72	69	73	0.0074	11
	part. alt.	11	0.26	31	27		
	altered	0	0	0	0		
OB-24	unaltered	23	1.12	40	29	0.0220	9
	part. alt.	14	0.92	25	24		
	altered	20	1.79	35	47		
OB-66	unaltered	5	0.14	31	16	0.0263	8
	part. alt.	5	0.15	31	17		
	altered	6	0.60	38	67		
OB-62	unaltered	16	0.48	11	12	0.0680	2
	part. alt.	79	1.61	53	42		
	altered	53	1.78	36	46		
OB-127	unaltered	35	1.00	74	79	0	12
	part. alt.	12	0.27	26	21		
	altered	0	0	0	0		
OB-70	unaltered	36	1.62	13	9	0.0279	7
	part. alt.	72	3.61	27	21		
	altered	159	12.12	60	70		
OB-25	unaltered	138	3.11	62	42	0.0284	6
	part. alt.	64	2.76	29	38		
	altered	21	1.47	9	20		
OB-115	unaltered	12	0.04	29	2	0.0987	1
	part. alt.	8	0.36	20	19		
	altered	21	1.47	51	79		
OB-29	unaltered	13	0.41	68	43	0.0663	3
	part. alt.	1	0.12	5	13		
	altered	5	0.42	26	44		
OB-98	unaltered	33	1.48	32	23	0.0298	5
	part. alt.	38	2.21	37	34		
	altered	33	2.75	32	43		

Table 3. Combined sample population statistics and PIXE/GUPIX *1118* analyses results.

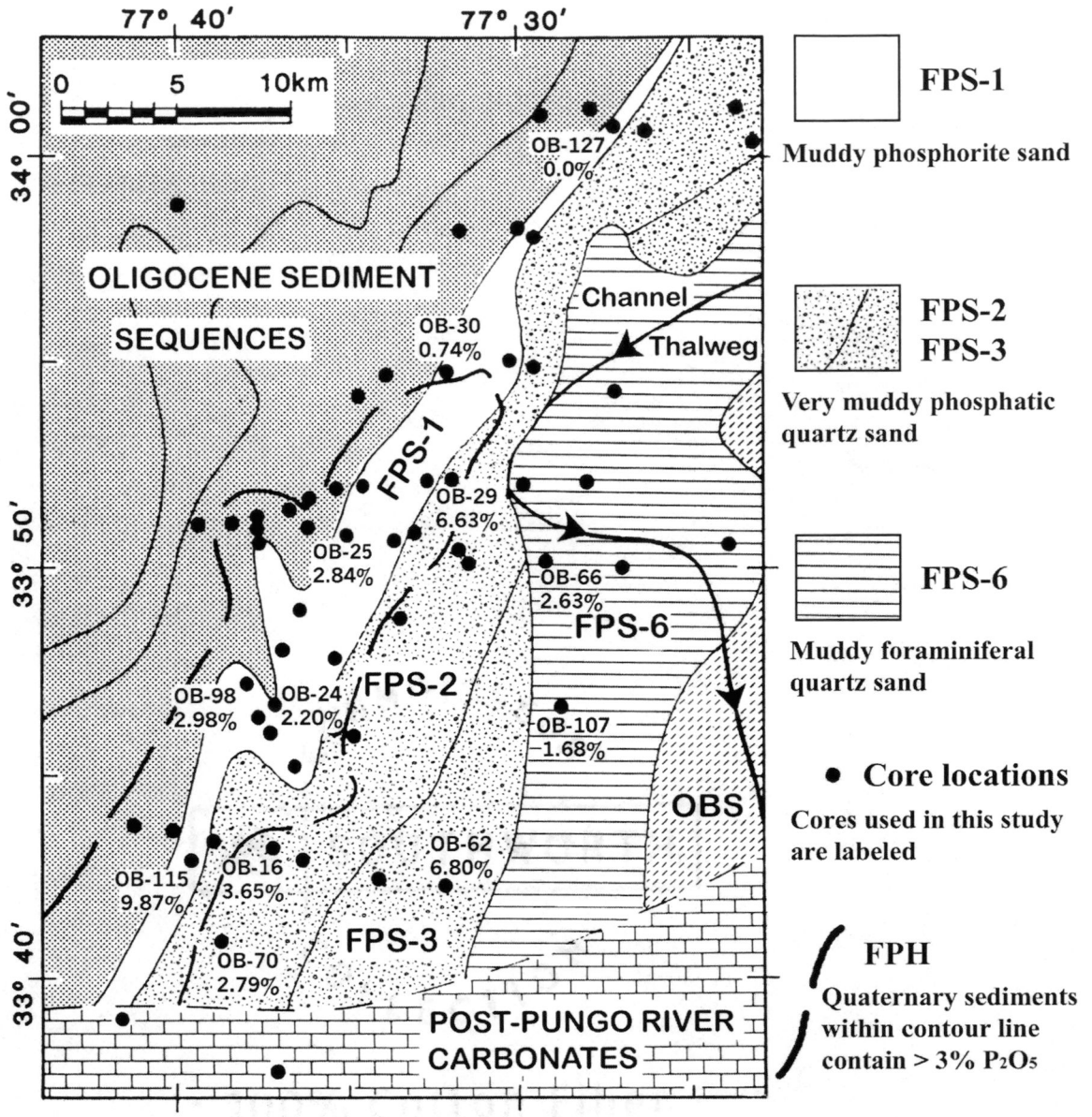

Figure 13. Map showing the iron concentrations produced by GUPIX for cores in Frying Pan phosphate district (modified from Riggs et al., 1985). Map base from Figure 6.

specimens, give OB-25 an iron signature of over 2.8%. OB-70 is composed of mostly altered and partially altered foraminifera, and is the largest sample in the study group both in terms of weight and numbers of tests; the iron signature from this sample is therefore anomalously low (2.7% Fe). In this sample, individual unaltered specimens are as heavy as partially altered specimens, which may contribute to lowering the iron signature of this sample. OB-66 is the smallest sample, has roughly equal numbers of tests in each alteration category, and slightly over 2.6% Fe. OB-24 has predominantly unaltered and partially altered tests, and produced a 2.2% Fe signature. OB-107 (approx. 1.7% Fe), OB-30 (0.74% Fe) and OB-127 (0.0% Fe) have low iron signatures that correlate with the numerical dominance of unaltered foraminifera.

Trace Elements

The *1013* analysis employed high beam intensity and a light-element x-ray absorber (0.05 mm aluminum filter #2) to capture counts from heavier trace elements. Results from *1013* were corrected for variable filter transmission, and GUPIX produced calcium ratios for the trace elements that exhibited significant peaks. It is clear from these results that some specimen tests contain small amounts of Zn and Sr (Appendix C-b). Some samples probably had Mn peaks, but fit errors of greater than 10% suggest that these results are unreliable. The control sample OB-24c (altered) produced a reliable Cu peak and a possible fit for Co. Although these samples were analyzed for twice as long, and with up to ten times the beam intensity as the other two analyses, it was not possible to accumulate significant counts for other trace elements. In summary, the detected occurrence of trace elements is too sporadic to reveal any meaningful patterns.

The appearance of Sc in a nearly constant ratio with Ca in the *1118* (and *1006*) analysis indicates it is the result of fit error on the tail of the Ca peak; however, GUPIX fit the Ca peak more appropriately when Sc was included in the unfiltered analyses. Using an x-ray absorber may have filtered out Sc in the *1013* analysis, but most likely allowed GUPIX to more precisely analyze the Ca peak.

Further testing with PIXE for extended periods of time, at higher beam intensity and with a light-element absorber in place, might reveal trace elements in detectable quantities in additional cores; Zn, Co and Cu were detected in some samples suggests that these elements are present in trace amounts.

DISCUSSION

Elemental analyses produced by PIXE and GUPIX in this study corroborate the microprobe results of Riggs et al. (1984) in that diagenetic alteration of selected Quaternary miliolids in cores from the Frying Pan phosphate district is primarily ferruginization. Iron concentrations in the foraminifera range from 0% to nearly 10% (Table 3). Trace elements were detected in some samples, but not consistently enough to establish any patterns.

Comparing percent Fe from PIXE analyses to the visually assessed degree of alteration for the study samples reveals that increasing iron concentrations generally correspond with increased number and/or weight of altered and partially altered foraminifera (Figs. 14 and 15). Although the number of altered specimens and weight percentages co-vary with increasing iron concentration, the relationship is imperfect; weight percentages correlate more closely.

Geochemical Data

Ellington (1984) performed inductively coupled argon plasma emission spectroscopy (ICAPES) on select phosphate grains from core locations in the Aurora and Frying Pan phosphate districts in order to determine general chemical differences between the grain morphologies. The ICAPES data for cores OB-24, -25, -29 and -30 are shown in Appendix D-a. ICAPES data for bulk-sediment samples taken at intervals from several cores in the Frying Pan phosphate district are presented in Appendix D-b (Mallette, 1986). Chemical analysis performed under industry standard wet chemical analytical

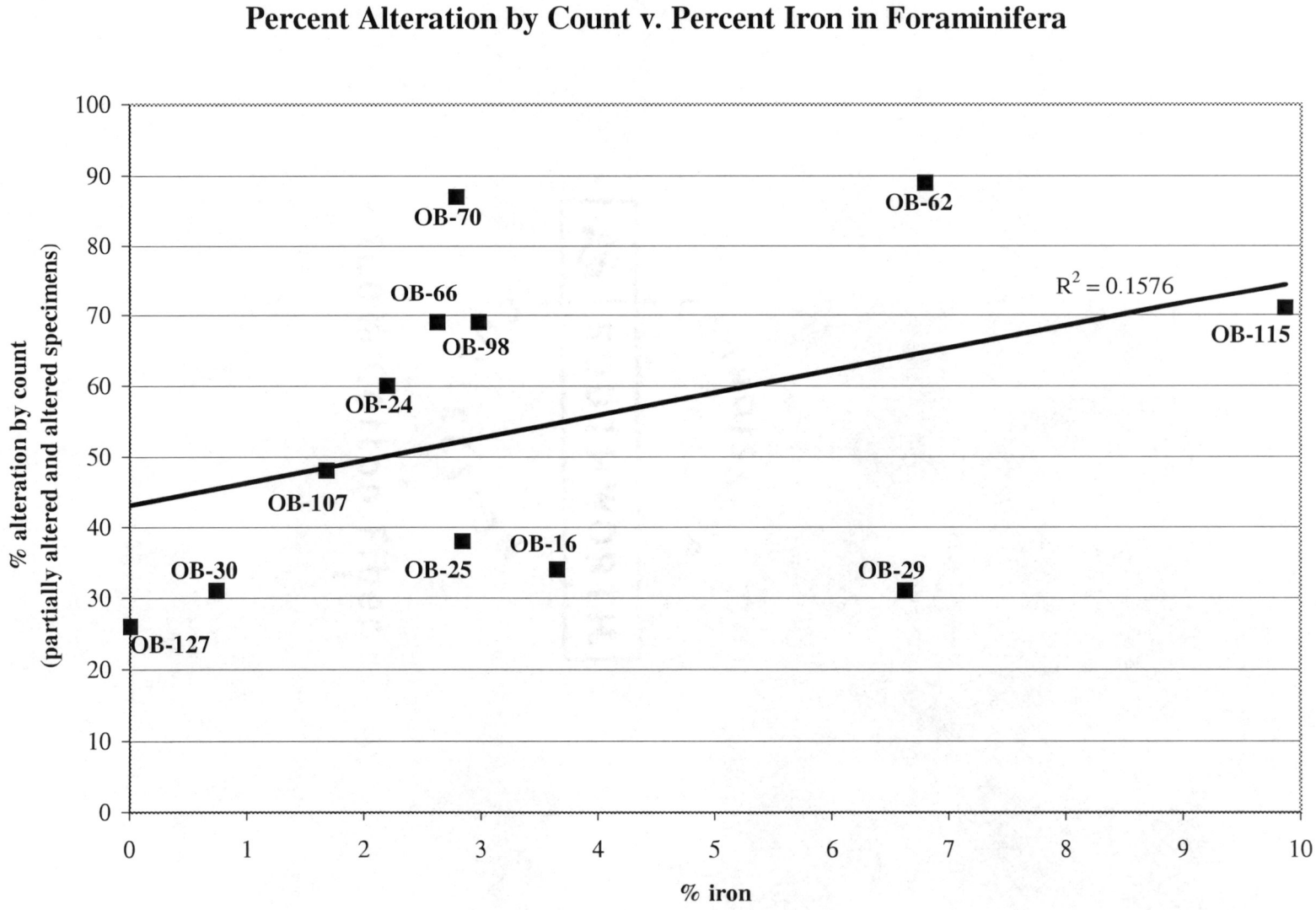

Figure 14. Comparison of percent alteration of foraminifera by test count to iron signatures in study samples.

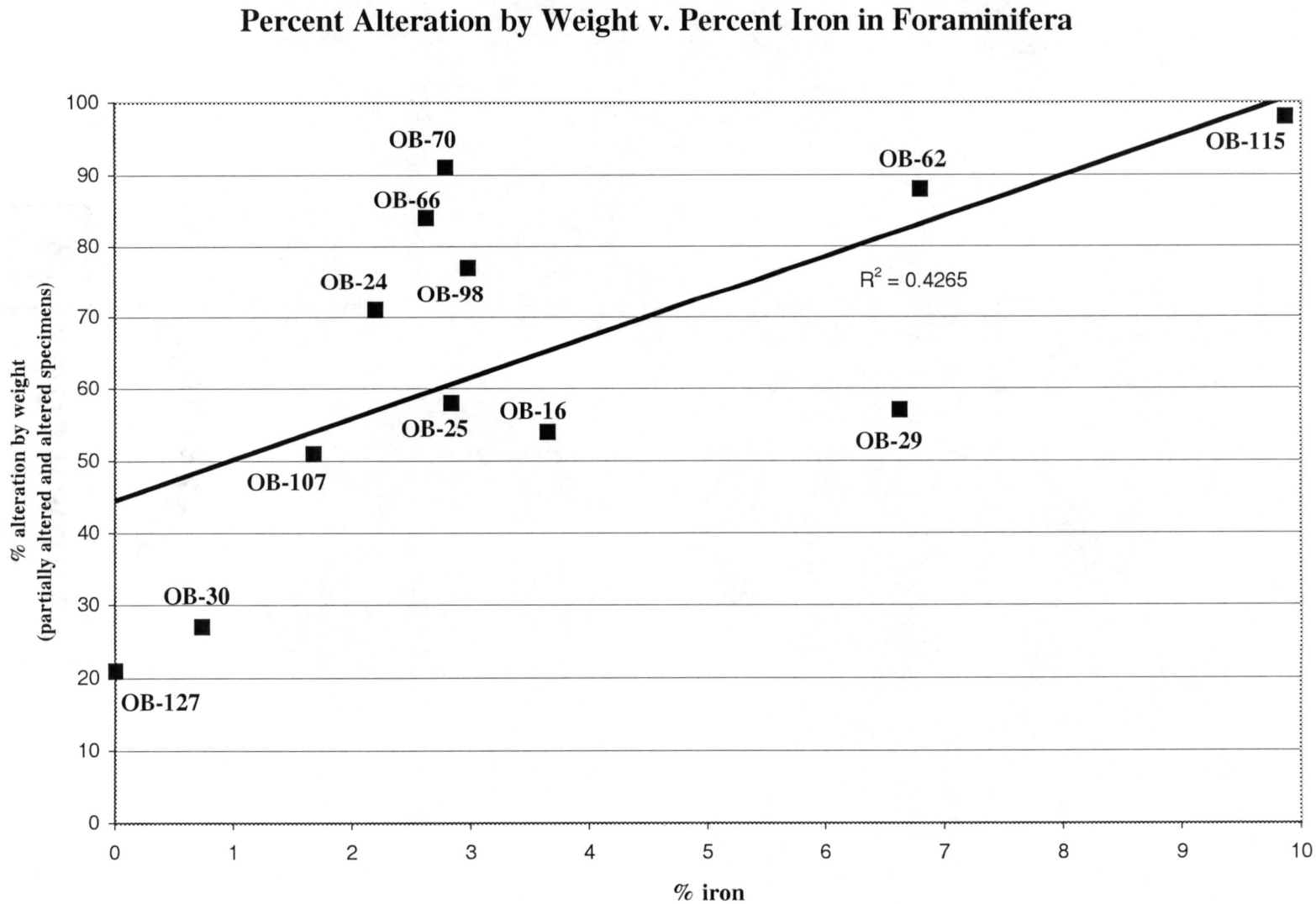

Figure 15. Comparison of percent alteration of foraminifera by mass to iron signatures in study samples.

techniques on multiple bulk-sediment samples and phosphate concentrates were used to define the mean chemical signatures of FPS-1 and FPH (Appendix D-c; Riggs et al., 1985). Handpicked phosphate concentrates from FPS-1 and FPH were also tested with ICAPES in the Riggs et al. (1985) study (Appendix D-c). These data will be used to characterize the Miocene and Quaternary sediments in the cores from which foraminifera were analyzed in this study.

Spatial Relationships

There is no simple relationship of ferruginization in foraminifera from Quaternary sediments with the types of underlying Miocene sediment (Fig. 13). Foraminifera from above the phosphorites of FPS-1 span the range of iron concentrations from 0 to 9.8%. Those above the siliciclastic muds of FPS-2 and -3 are relatively iron-rich (2.7-6.8% Fe), whereas those above FPS-6 are somewhat lower (1.7-2.6% Fe). Percentages of iron in foraminifera are generally high in the area enclosed by the 3% P_2O_5 contour, but some samples within this area are rather low (e.g., OB-24) and a few samples outside this area are iron-rich (e.g., OB-62 and -16).

The core with the highest iron signature, OB-115, was recovered from the southern extent of seismic unit FPS-1, the most phosphatic Miocene unit, within the FPH 3% P_2O_5 contour (Fig. 13). OB-115 was not included in the geochemical work by Ellington (1984) or Mallette (1986), so no direct comparison with P_2O_5 or Fe_2O_3 content in the underlying Miocene sediment can be made.

Visual assessment of test alteration from OB-62, and their subsequent PIXE analysis confirm a high degree of ferruginization (nearly 7%) (Table 3). The core was recovered

from an erosional outlier in FPS-3, a slightly sandy (5%) mud (Figs. 2 and 8), which contains bulk sediment concentrations of 1.60-1.93% P_2O_5 and 2.77-3.16% Fe_2O_3 that generally increase with depth (Appendix D-b; Mallette, 1986). Modest P_2O_5 content coupled with relatively high iron content suggests that the phosphatic muds of FPS-3 may be a source for iron product found in the Quaternary foraminifera from this core.

OB-29 was recovered from within the FPH 3% P_2O_5 contour line, near the delineated boundary of FPS-2 and the more phosphatic FPS-1 (Fig. 6), and penetrates FPS-1 sediments around 6 m below the surface. OB-29 is also located near the geographical center of the Frying Pan phosphate district, where phosphate concentrations are highest in the underlying Miocene sediments. Phosphate pellets in this core yield concentrations of 28.5-29.3% P_2O_5 and 0.40-0.76% Fe_2O_3; the intraclast analyzed from this core was slightly more phosphatic (29.9 P_2O_5, 0.41 Fe_2O_3) (Ellington, 1984; Appendix D-a). Mallette (1986) reported bulk-sediment concentrations of P_2O_5 (0.77-6.94%) that increase with depth, and Fe_2O_3 (0.34-1.51%) concentrations that are highest around 3 m from the surface (Appendix D-b). High P_2O_5 and modest iron content suggest that the phosphate grains are the primary iron source for ferruginization of the foraminifera.

Iron signatures in the foraminifera from OB-16 are relatively high (3.65%) (Table 3). OB-16 was recovered from an erosional outlier in FPS-2, a slightly phosphatic sandy mud unit, just east of the FPH 3% P_2O_5 contour (Fig. 13). Bulk sediment P_2O_5 concentrations in OB-16 (0.88-1.21%) are the lowest tested by Mallette (1986), but Fe_2O_3 concentrations are among the highest (4.78-5.27%) (Appendix D-b). As with OB-62, the

phosphatic muds (here of FPS-2) contain concentrations of iron that may contribute to precipitates in the foraminifera.

Miliolids from OB-98 were nearly evenly split between the alteration categories, and produced an iron signature of close to 3.0% (Table 3). OB-98 penetrated an erosional outlier of FPS-2 near the geographic center of the phosphate district (Fig. 13). P_2O_5 concentrations in bulk sediment samples decrease with depth in OB-98 (1.53% at 1.25 m depth to 1.00% at 4.0 m depth); conversely, concentrations of Fe_2O_3 increase with depth (2.82-3.48%) (Mallette, 1986; Appendix D-b). The moderately high concentrations of P_2O_5 and Fe_2O_3 in this core correlate to others recovered from FPS-2 (e.g., OB-16 and -62), and again indicate the mud to be a source of iron product in foraminiferal tests.

OB-25, with a majority unaltered specimens, was recovered from the updip limit of the Miocene sediments and penetrated less than 1.5 m of FPS-1 before encountering Oligocene sediments. Concentrations of P_2O_5 in pellets from OB-25 increase with depth from the surface (27.9%) to 1.0 m deep (28.3%), whereas Fe_2O_3 concentrations decrease with depth from 1.14 to 0.62% (Ellington, 1984; Appendix D-a). The iron signature detected in foraminifera from the Quaternary sands is relatively low (approx. 2.8%), considering the location of OB-25 within the FPH 3% P_2O_5 contour, and is likely the result of the minimal thickness of phosphate-bearing sediments in the core, and its proximity to the updip limit of the Miocene.

The iron concentration in OB-70 (approximately 2.8%), which penetrates FPS-2, is roughly comparable to concentrations in OB-16 and -98, which also penetrate the phosphatic mud unit. The slightly lower iron content in foraminifera from the Quaternary

sands of this core may be attributable its location in the southern extent of the study area (Fig. 13). OB-70 was not among the cores analyzed by the previous geochemical studies in Frying Pan phosphate district. However, as with OB-62, -16 and -98, the phosphatic muds appear to be a likely source for iron that precipitates in the foraminiferal tests.

OB-66 is one of two cores that penetrate FPS-6, a channel fill facies of foraminiferal quartz sand, the least phosphatic Miocene unit in the Frying Pan phosphate district. The smallest sample in the study group, OB-66 produced an iron signature of 2.63% (Fig. 13). Bulk sediment analysis of OB-66 reveals FPS-3 sediments in the core at 3.5 m depth that contain small concentrations of P_2O_5 (1.77%) and Fe_2O_3 (1.65%) (Mallette, 1986; Appendix D-b). The presence of FPS-3 sediments at this depth may be the source of the iron product in the foraminiferal tests.

Mallette (1986) described bulk sediment P_2O_5 concentrations that increase from 9% at the surface to 23% at 1 m depth in OB-24; these concentrations are higher than any other concentrations reported in southern Onslow Bay (Appendix D-b). Iron concentrations were low in the foraminifera (0.74%) and in the bulk sediment (0.58-0.99% Fe_2O_3) (Mallette, 1986), despite a small majority of partially altered and altered specimens (Table 3). The core was recovered from FPS-1 near the Miocene updip limit and only penetrated 1.6 m of the Pungo River Formation (Fig. 13). As with OB-25, the limited thickness of FPS-1 in this core and its proximity to the updip limit of FPS-1 may contribute to the low extent of alteration of miliolids in the Quaternary sands, because the underlying rich pelletal phosphorites seem to be a likely source of iron in FPS-1.

The foraminifera analyzed from OB-107, recovered from the foraminiferal quartz unit FPS-6, have a low Fe signature (approx. 1.7%) that parallels the numerical importance of visually unaltered specimens (Fig. 13). Iron content in bulk sediment samples from OB-107 is high (4.24-4.54% Fe), and P_2O_5 is average (1.19-1.46%); both show a general increase with depth (Mallette, 1986; Appendix D-b). OB-107 penetrated less than 3 m of the Pungo River Formation before entering Oligocene strata; again, this limited thickness of Miocene sediment may be the cause of the low iron signature in the foraminifera from the Quaternary sands.

OB-30 and -127 lack altered foraminifera, which corresponds with the little to no iron signature produced during the PIXE analyses. These cores were recovered from FPS-1 near the northern extent of the phosphate district and well removed from the richest Miocene phosphorites. Bulk sediment analyses for OB-30 are not available; a phosphate pellet analyzed from this core had a moderate P_2O_5 (28.5%) concentration and a low 0.37% Fe_2O_3 (Ellington, 1984; Appendix D-a). Bulk sediment P_2O_5 and Fe_2O_3 values in OB -127 are comparable to cores where the percent iron in foraminifera is higher (Appendix D-b). At OB-127, the FPS-1 outcrop belt is very narrow, and little iron may be mobilized from it.

Geochemical Trends

Pellets are the dominant phosphate morphology in the Frying Pan phosphate district. Phosphate pellets from the top 1.5 m of Miocene sediment in core OB-24, -30, -25, and -29 were analyzed for weight percent of P_2O_5 and Fe_2O_3 (Ellington, 1984; Appendix D-a). Pellets from only two cores were analyzed from the deeper section of the cores (1.5-7.2

m), making it difficult to define geochemical changes with depth in the cores. In general, iron content in foraminifera increases in relation to both the P_2O_5 and Fe_2O_3 concentrations in phosphate pellets from the top 1.5 m of the cores analyzed (Figs. 16 and 17). However, only Fe_2O_3 concentrations in the phosphate pellets show a statistically significant relationship with ferruginization of miliolids from overlying sediments. Trends in P_2O_5 and Fe_2O_3 for phosphatic intraclasts are impossible to determine in the six samples from the two cores that were analyzed.

Analyses of bulk sediment show a negative co-variation between the weight percentage of P_2O_5 in the top 2 m of sediment from cores OB-127, -107, -24, -98, -16, -29 and -62, and iron concentrations in foraminifera from these cores (Fig. 18; Mallette, 1986). This trend is also seen in the deeper (2-5 m) sections of the cores (Fig. 19). The co-variation is reversed at depth (5-7.5 m). The paucity of altered specimens in OB-127, and therefore iron concentration, skews the trendlines comparing Fe concentrations in the specimens to the bulk sediment analyses; if the outlying OB-127 were to be removed from the comparison, the co-variation would be more strongly positive for all depths.

There is an increased concentration of Fe_2O_3 with depth in the cores analyzed by Mallette (1986). Depletion of iron from bulk sediment samples in the top 1 m of Miocene sediment parallels an increase in iron content in the foraminifera from these cores (Fig. 20); this correlation is decreased with depth in the core (Fig. 21). The correlations between bulk sediment P_2O_5 and Fe_2O_3 weight percentages and the degree of ferruginization in the Quaternary miliolids are statistically insignificant at all depths.

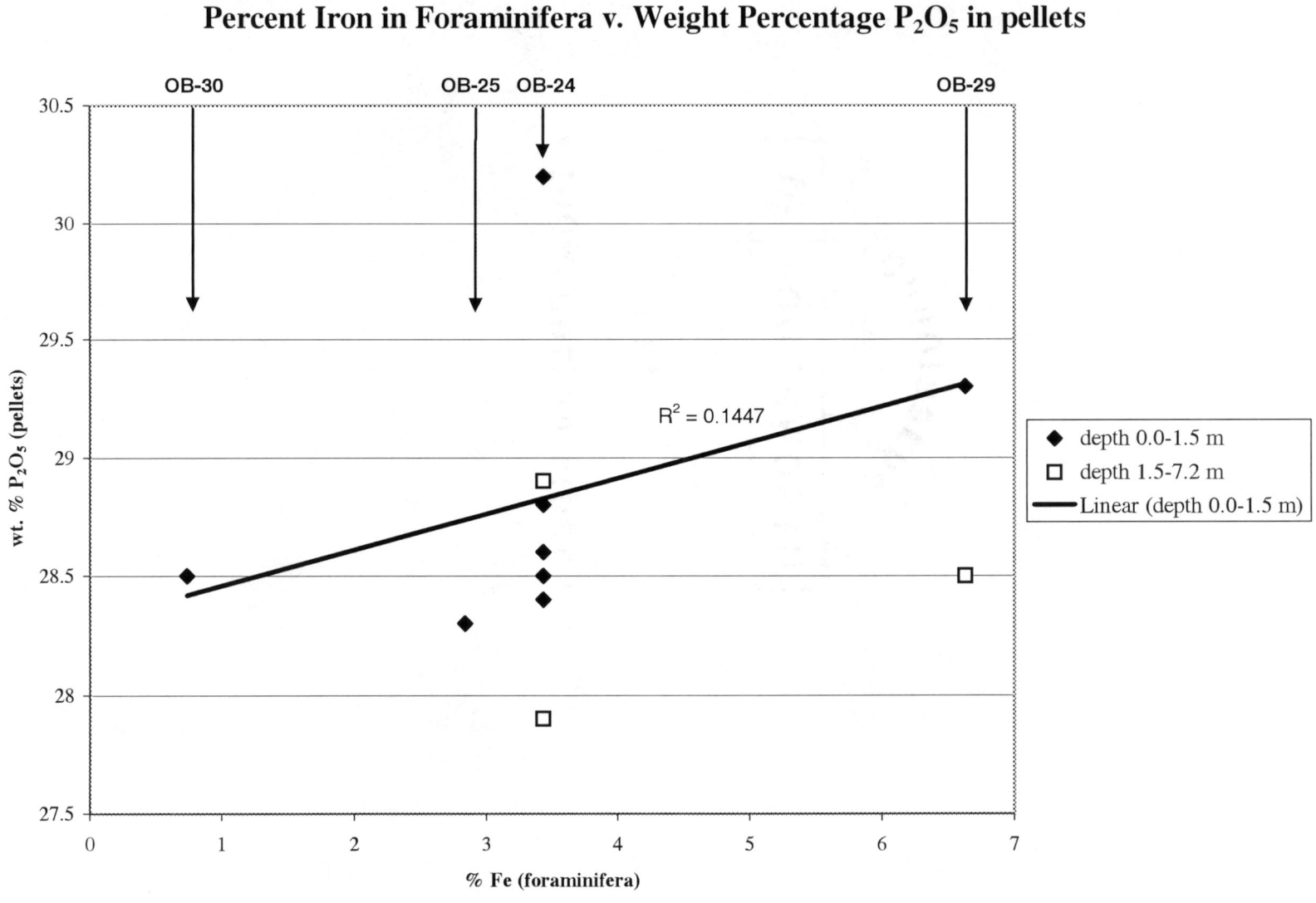

Figure 16. Comparison of weight percentage P_2O_5 in pellets and iron signatures in foraminifera from OB-30, -29, -25 and -24.

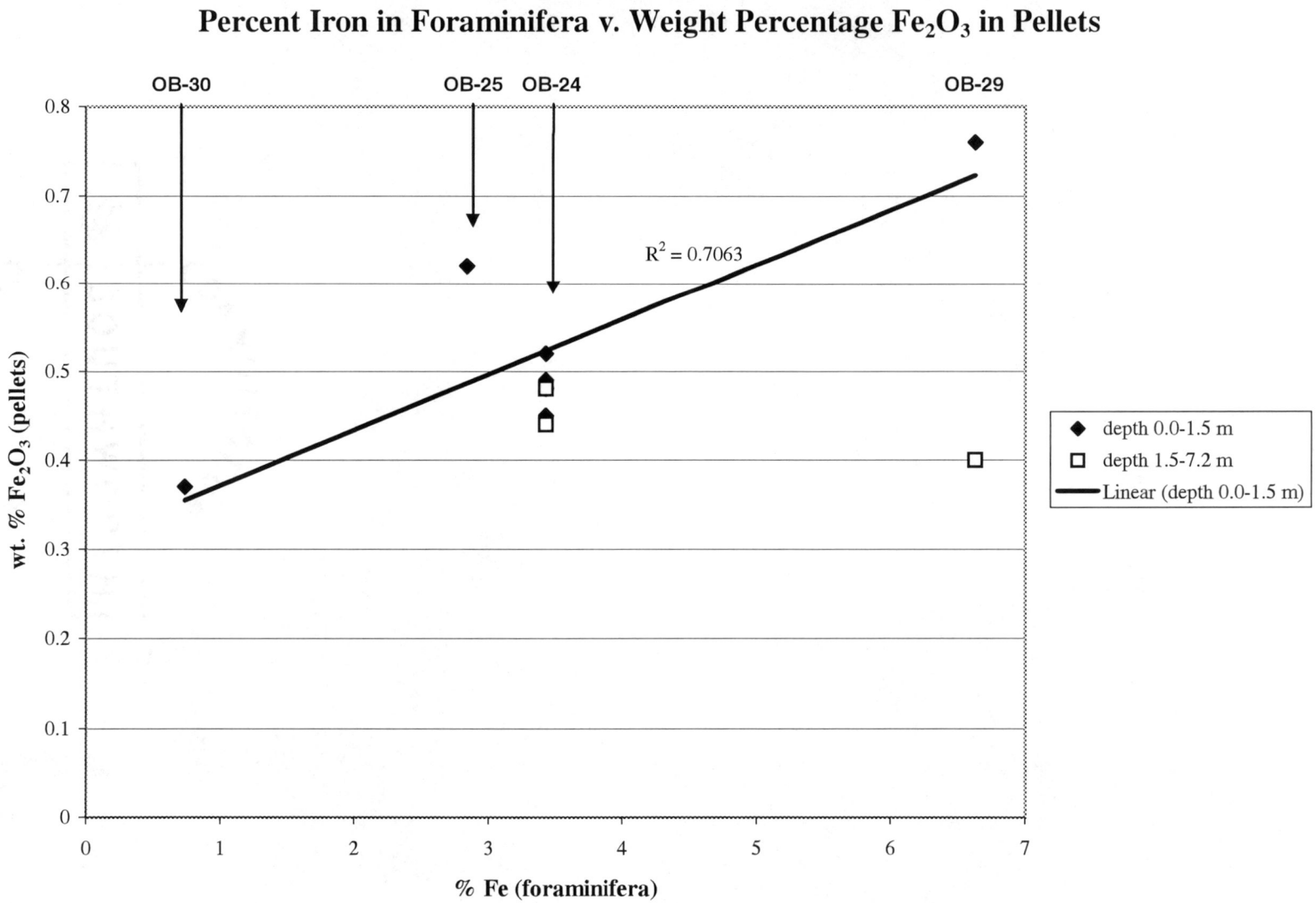

Figure 17. Comparison of weight percentage Fe_2O_3 in pellets and iron signatures in foraminifera from OB-30, -29, -25, and -24.

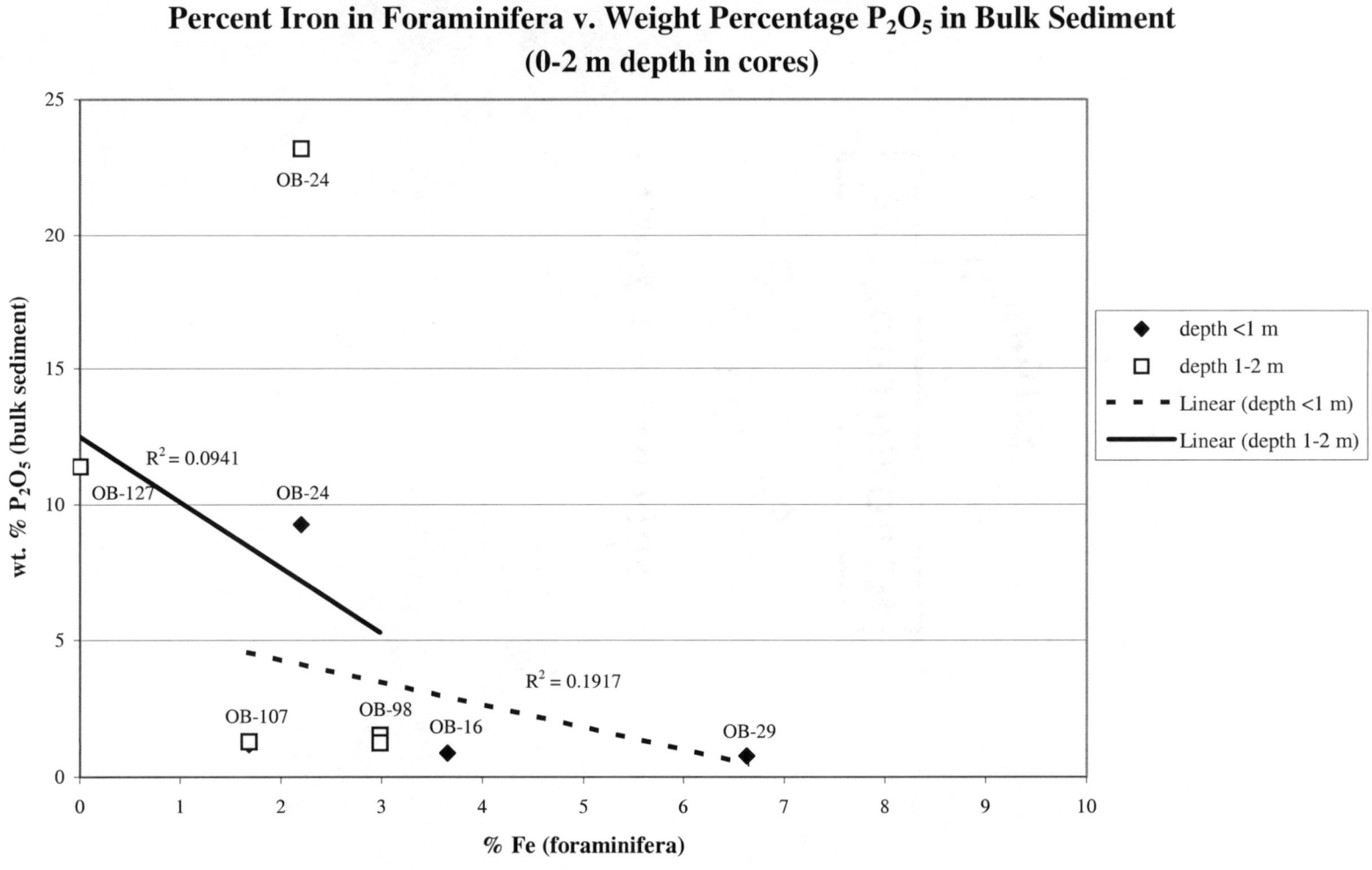

Figure 18. Plot of bulk sediment P_2O_5 and iron signatures in foraminifera from OB-127, -107, -24, -98, -16, and -29, and separated by depth in core.

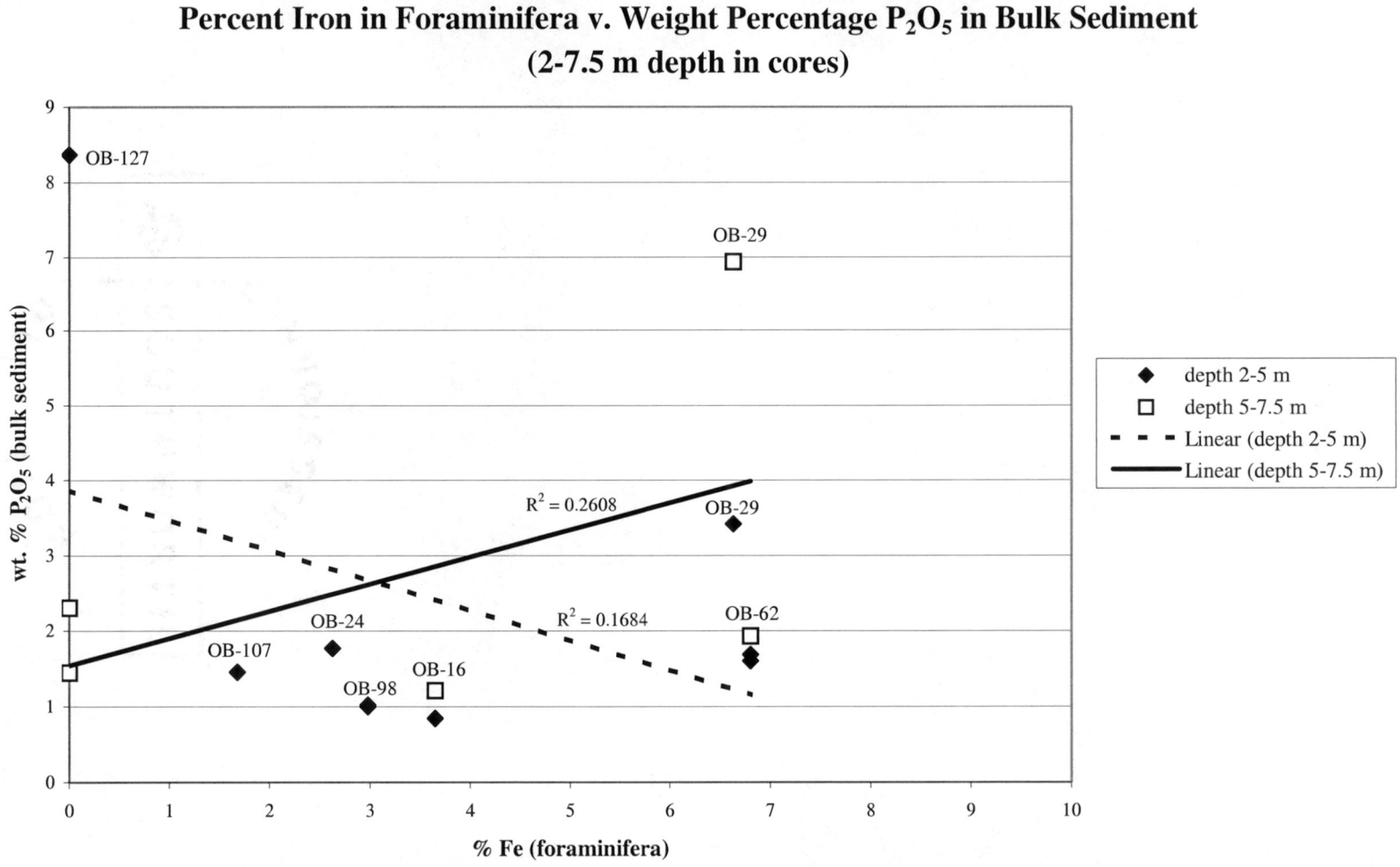

Figure 19. Plot of bulk sediment P_2O_5 and iron signatures in foraminifera from OB-127, -107, -24, -98, -16, -29 and -62, and separated by depth in core.

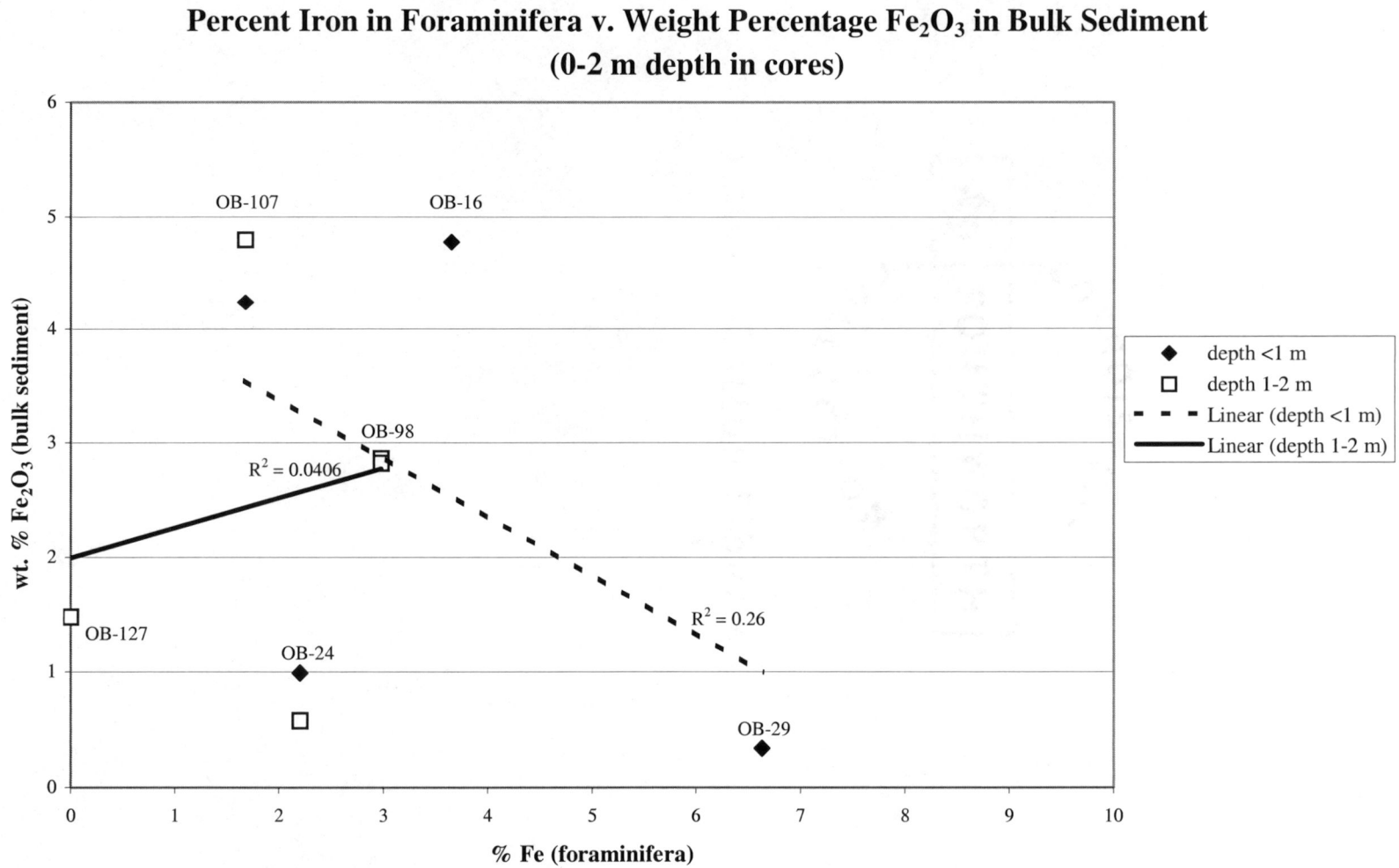

Figure 20. Plot of bulk sediment Fe_2O_3 and iron signatures in foraminifera from OB-127, -107, -24, -98, -16 and -29, and separated by depth in core.

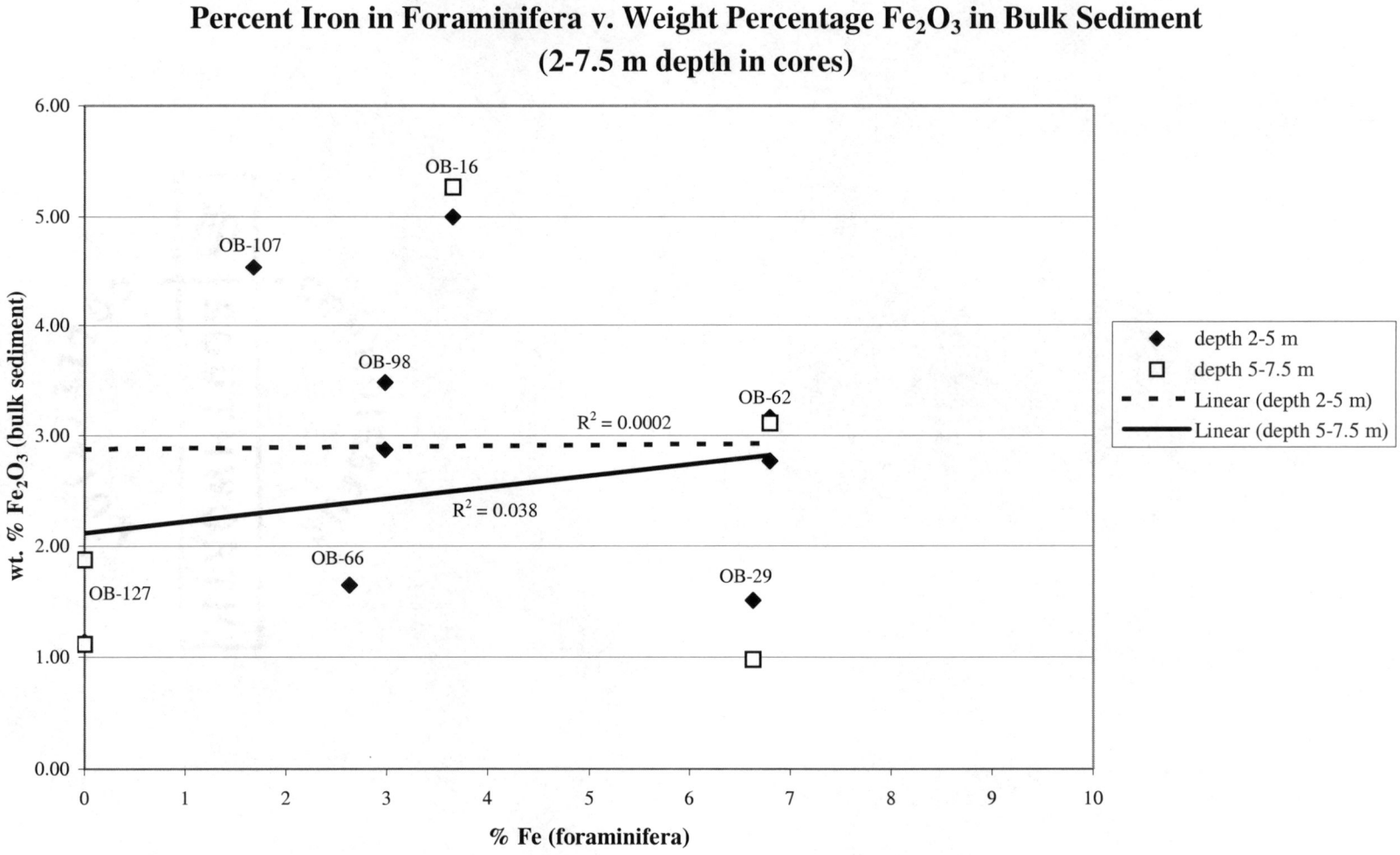

Figure 21. Plot of bulk sediment Fe_2O_3 and iron signatures in foraminifera from OB-127, -107, -24, -98, -16, -29 and -62, and separated by depth in core.

Riggs et al. (1985) grouped phosphate concentrates, and bulk sediment samples, as either originating from Miocene sediments (FPS-1) or the overlying Quaternary sand (FPH) (Appendix D-c). Analyses of these grouped samples indicate a significant increase in the concentration of Fe_2O_3, and a slight decrease in the concentration of P_2O_5, in FPH as compared to the underlying FPS units (Fig. 22 and 23, respectively). Analysis of a single phosphate pellet collected from the top 0.5 m (FPH) of OB-25 supports this trend, with a relatively high Fe_2O_3 concentration (1.14%) in comparison to samples from FPS-1 (0.62%) in this core (Appendix D-a; Ellington, 1984). These relationships suggest that iron is mobilized at much higher rates than phosphorus, which is consistent with: 1) ferruginization dominating over phosphatization as an alteration process on Quaternary foraminifera; 2) the presence of a source for iron (likely the muds of FPS-2 and –3, or the immediately underlying phosphorite sediments in these cores) in addition to pelletal phosphorites; and 3) perhaps also the significantly increased iron content in surface sediments and phosphate grains.

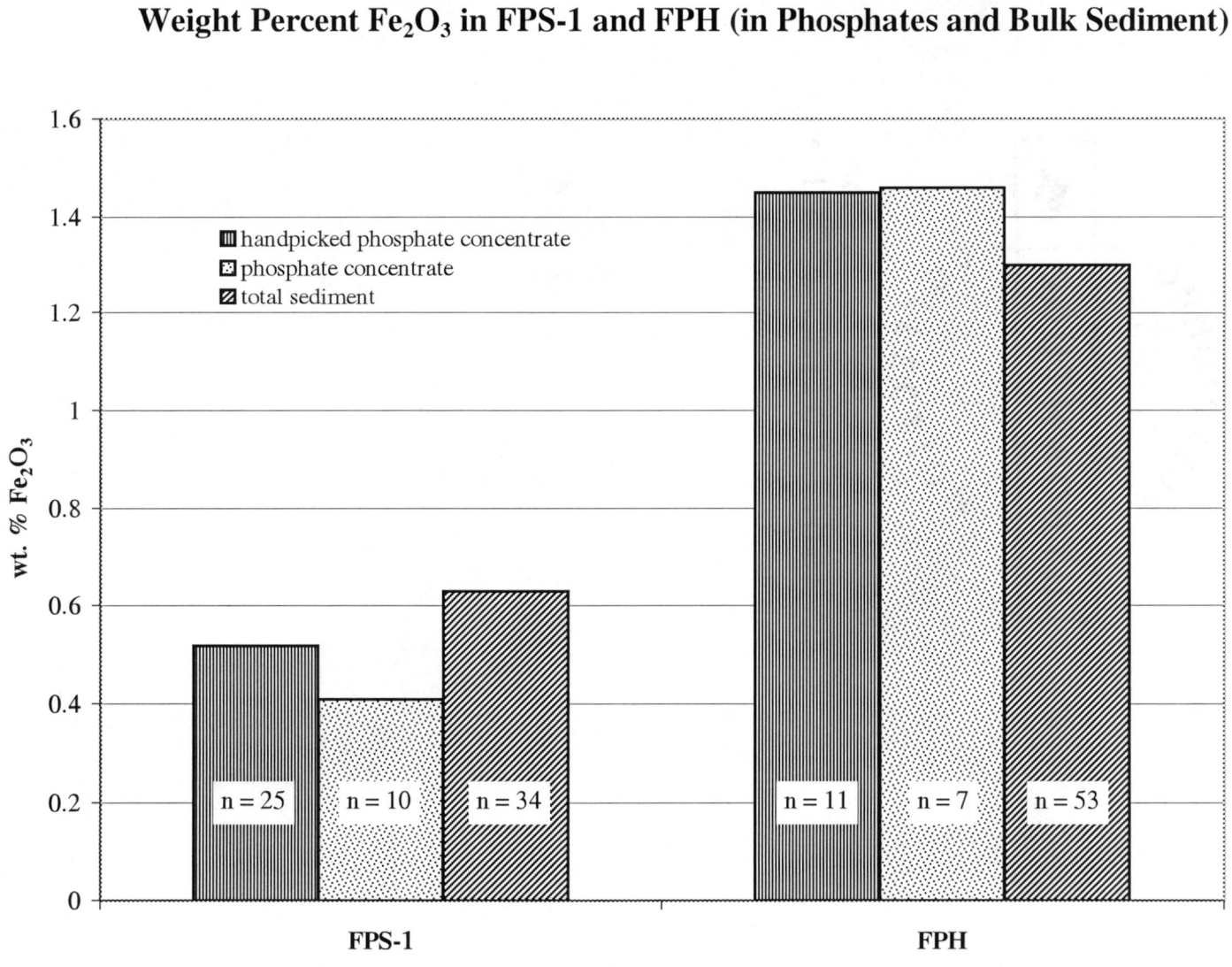

Figure 22. Weight percentage Fe_2O_3 in phosphate concentrates and bulk sediment from FPS-1 and FPH.

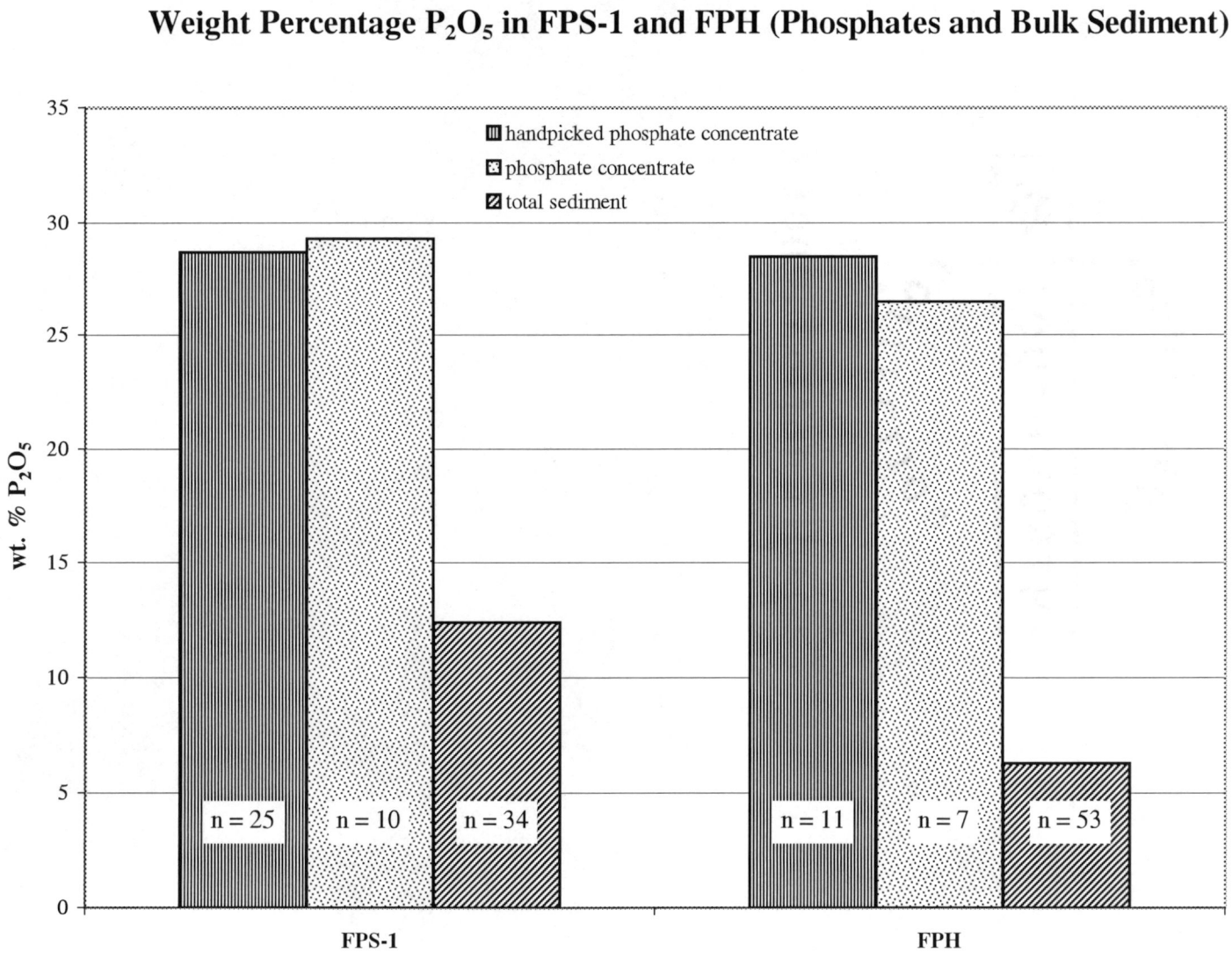

Figure 23. Weight percentage P_2O_5 in phosphate concentrates and bulk sediment from FPS-1 and FPH .

CONCLUSIONS

The alteration of foraminiferal tests in Quaternary sediments of the Frying Pan phosphate district in southern Onslow Bay is, as postulated by Riggs et al. (1984) on the basis of microprobe analyses of a few specimens, largely a process of ferruginization. Proton induced x-ray emission (PIXE) spectrometric analyses demonstrate that alteration to iron dominates across the study area. PIXE spectrometry and elemental yield calculations performed by GUPIX on foraminifera in various stages of alteration show an increase in iron concentration that parallels discoloration of the tests. To estimate the scale of alteration, PIXE spectrometry is more reliable than simple counts of discolored specimens because the actual scale of ferruginization is a function of specimen mass as well as numerical abundance.

Miliolid foraminifera have high magnesium (> 4% Mg) calcite tests (Loeblich and Tappan, 1988). Although other minerals (e.g., Mg, Fe) can substitute for Ca^{+2} in the tests of foraminifera, $CaCO_3$ is typically stable at most temperatures and pressures (Berry and Mason, 1959). High magnesium calcite is more chemically unstable, and iron precipitation often occurs in skeletons of this composition without destruction of the original test structure (Richter and Fuchtbauer, 1978). Fe^{+2} more readily substitutes for Mg than for Ca^{+2} because their ionic radii are more similar (Fe^{+2} = 0.74; Mg = 0.66; and Ca = 0.99; Berry and Mason, 1959). Among the foraminifera present in surface sediments of the study area, members of the family Miliolidae are preferentially

ferruginized and so provide a reliable measure of diagenetic alteration in the Quaternary sands of Onslow Bay.

In general, the highest Fe signatures are produced by Quaternary foraminiferal samples collected from cores that penetrated Miocene seismic units FPS-1 and FPS-2 within the FPH 3% P_2O_5 contour area. Samples collected from Quaternary sands overlying unit FPS-6, and those collected from the northern extent of the Frying Pan phosphate district, contain the lowest Fe signatures. However, there is no simple spatial relationship between the extent of ferruginization among Quaternary foraminifera and the lithology/mineralogy of the immediately underlying fourth-order Miocene sequence. For example, core OB-62, which overlies FPS-3, has the second highest iron content of the foraminiferal samples; the FPS-1 phosphorites located at depth in those cores that penetrated FPS-2 and -3 muds may contribute to iron product that precipitates in the foraminiferal tests. Relatively high iron content combined with low phosphate weight percentages in bulk sediment samples from FPS-2 and -3 (Mallette, 1986) suggests that these muds also contain iron-rich minerals (iron oxides and iron sulfides). Conversely, the percent iron is anomalously low in core OB-24, which penetrates phosphorites of FPS-1 in the heart of the area defined by the FPH 3% P_2O_5 contour; the limited thickness of phosphate-bearing sediments, and more importantly the location of this core near the updip limit of Miocene phosphate-bearing sediments, may have restricted iron production in this instance.

The miliolids collected for this study were recovered from the thin and mobile Quaternary sand sheet that discontinuously overlies the Miocene sediments in southern

Onslow Bay. Direct correlations between spatial distribution of ferruginized miliolids and nature of the immediately underlying Miocene unit in the recovered core are complicated by the probability that the miliolids were transported during high-energy events after diagenesis. However difficult the spatial correlations may be to discern, the presence of ferruginized foraminifera over an area of iron-rich phosphate deposits and muds suggests vertical dissemination of iron product.

Sources

Comparison of iron concentrations in miliolid foraminifera to geochemical data for the underlying phosphatic units of the Miocene Pungo River Formation and the surrounding Quaternary sands suggests that the ferruginization of the foraminifera is related to the iron component of the phosphate, which decreases towards the top of the Miocene sediments and increases in the overlying sands. Phosphate pellets can contain numerous mineral phases that incorporate iron, which may leach out during reworking of the pellets. Etching of phosphate pellets from FPS sediments revealed silt-sized quartz, pyrite, diatom fragments and clay minerals (Mallette, 1986). Ellington (1984) reported high Fe loading in phosphate pellets from the Frying Pan phosphate district that suggests the presence iron sulfides. Pyrite is commonly associated with phosphate pellets from the Aurora phosphate district, which may have had a depositional environment similar to that of FPS pelletal phosphates (Ellington, 1984).

Another possible source of iron that contributes to the alteration of foraminifera in Quaternary sediments is the phosphatic muds in fourth-order seismic sequences FPS-2 and FPS-3. Bulk sediment samples from cores recovered from these units are high in

Fe_2O_3, but relatively depleted in P_2O_5 (Mallette, 1986). The phosphorite sands of FPS-1 are found between 3 and 6 meters deep in cores taken from FPS-2, -3 and -6 sediments (Snyder et al., 1988), which may contribute to the high iron concentrations in these sediments given a method of vertical dissemination of iron product. Trace amounts of pyrite are also documented in the mud facies of the Frying Pan phosphate district (Ellington, 1984).

Mechanisms

Groundwater seeps in the vicinity of iron-bearing phosphates of Onslow Bay may provide a mechanism for the dissolution, vertical dissemination and precipitation of iron product from Miocene sediments into the overlying Quaternary miliolids. Iron has a very low solubility in seawater, and exists in extremely low concentrations (1 nmol per L Fe); ferrous iron would be absent during early diagenesis in the presence of reducing organic matter (Richter and Füchtbauer, 1978). Nutrient-rich groundwater discharges at a rate of 8-12 ml/m^2/minute from seeps located approximately 120 km offshore at a depth of 20 m in Onslow Bay (Merchant et al., 1996). The test chambers of Miocene foraminifera in the Frying Pan phosphate district are commonly infilled with Na-poor clinoptilolite and pyrite; the reduced Na content of the clinoptilolite fill, relative to K, suggests the mineral structure was flushed with fresh water (Moretz, 1988).

It is suggested here that as groundwater interacted with iron sulfides in the phosphate grains (iron sulfides and iron oxides in the mud units) of the Frying Pan phosphate district, the pH of the groundwater would drop as S^{-2} oxidized to SO_4, and iron is leached out of the phosphates as aqueous Fe^{+2}. At the sediment-water interface, the groundwater

is oxidizing (pH ~ 8); the aqueous Fe^{+2} component of the groundwater would precipitate (or oxidize to Fe^{+3}) within a very short distance of its outflow into the ambient seawater.

This mechanism may also contribute to the elevated iron content of the mud units of the Frying Pan phosphate district. Charette and Sholkovitz (2002) reported iron oxide staining on sediments overlying iron-rich groundwater seeps that form as a result of the oxidization of ferrous iron near the groundwater-seawater interface. Ferrous iron derived from clays in shale beds and volcanic ash bands have been correlated with the formation of ferroan calcite cement (Richter and Füchtbauer, 1978).

In the Frying Pan phosphate district, the Quaternary high-Mg miliolid foraminiferal tests undergo ferruginization that is likely related to the replacement of Mg by Fe^{+2} leached (by groundwater) from iron sulfides (e.g., pyrite) in the underlying Miocene phosphate grains, and perhaps also iron oxides in the mud facies. This phenomenon occurs because of the juxtaposition of an iron source (Miocene phosphates), grains susceptible to alteration (high-magnesium miliolid foraminifera in the immediately overlying Quaternary sands), and an environment where agents that dissolve iron (fresh water seeps) come into contact with an environment conducive to precipitation of Fe^{+2} (the marine sediment-water interface).

REFERENCES CITED

Berry, L. G. and Mason, B., 1959, Mineralogy: Concepts, Descriptions, Determinations: W.H. Freeman and Company, San Francisco, 630 p.

Boersma, A., 1978, Foraminifera: *in* Introduction to Marine Micropaleontology, Haq, B. U. and Boersma, A. (eds.), Elsevier, New York, p. 19-78.

Boyle, E. A., 1981, Cadmium, zinc, copper, and barium in foraminifera tests: Earth and Planetary Science Letters, v. 53, p. 11-35.

Boyle, E. A., 1988, Cadmium: Chemical tracer of deepwater paleoceanography: Paleoceanography, v. 3, p. 471-489.

Boyle, E. A., 1995, Limits on benthic foraminiferal chemical analyses as precise measures of environmental properties: Journal of Foraminiferal Research, v. 25, p. 4-13.

Brown, P. M., 1958, The relation of phosphorites to ground water in Beaufort County, North Carolina: Economic Geology, v. 53, p. 85-101.

Charette, M. A., and Sholkovitz, E. R., 2002, Oxidative precipitation of groundwater-derived ferrous iron in the subterranean estuary of a coastal bay: Geophysical Research Letters, v. 29, n. 10, p. 85 (1-4).

Culver, S. J., 1993, Foraminifera: *in* Fossil Prokaroyotes and Protists, Lipps, J. H. (ed.), Blackwell Scientific Publications, Inc., Cambridge, p. 203-248.

Ellington, M. D., 1984, Major and trace element composition of phosphorites of the North Carolina continental margin: M.S. Thesis, Department of Geology, East Carolina University, Greenville, NC, 93 p.

Fogle, M. R., 2000, The determination of trace element imbalances induced by neoplastic disease with proton induced x-ray emission spectroscopy (PIXE): M.S. Thesis, Department of Physics, East Carolina University, Greenville, NC, 135 p.

Gibson, T. C., 1983, Stratigraphy of Miocene through lower Pleistocene strata of the United States central Atlantic coastal plain: Smithsonian Contribution to Paleobiology, n. 53, p. 35-80.

Haynes, J. J., 1981, Foraminifera: John Wiley and Sons, New York, 433 p.

Johansson, S. A. E., Campbell, J. L., and Malmqvist, K. G., 1995, Particle Induced X-ray Emission Spectrometry (PIXE): *in* Chemical Analysis: A Series of Monographs on Analytical Chemistry and Its Applications, 133, J. Wiley and Sons, Inc., New York, 451 p.

Loeblich, A.R. and Tappan, H., 1988, Foraminiferal General and Their Classification: Van Nostrand Reinhold, New York, 970 p. plus 847 plates.

Mallette, P. M., 1986, Lithostratigraphic analysis of cyclical phosphorite sedimentation within the Miocene Pungo River Formation, North Carolina continental shelf: M.S. Thesis, Department of Geology, East Carolina University, Greenville, NC, 155 p.

Maxwell, J. A., Teesdale, W. J., and Campbell, J. L., 1995, The Guelph PIXE software package II: Nuclear Instructions and Methods in Physics Research, B95, p. 407-421.

Merchant, S. P., Snyder, S. W., and Evans, D. G., 1996, Modeling constraints on the origin of submarine groundwater discharge on the North Carolina continental shelf: Abstracts with Programs - Geological Society of America, v. 28, n. 2, p. 38.

Miller, J. A., 1982, Stratigraphy, structure and phosphate deposits of the Pungo River Formation of North Carolina: North Carolina Department of Natural Resources Comm. Devel., Geological Survey Bulletin 87, 32 p.

Moretz, L. C., 1988, Diagenesis of benthic foraminifera in the Miocene Pungo River Formation of Onslow Bay, North Carolina continental shelf: M.S. Thesis, Department of Geology, East Carolina University, Greenville, NC, 94 p.

Richter, D. K., and Füchtbauer, H., 1978, Ferroan calcite replacement indicates former magnesian calcite skeletons: Sedimentology, v. 25, p. 843-860.

Riggs, S. R., 1984, Paleoceanographic model of Neogene phosphorite deposition, U.S. Atlantic Continental Margin: Science, v. 223, n. 4632, p. 189-204.

Riggs, S. R., Snyder, S. W., and Spruill, R. K., 1984, Ferruginization and phosphatization of foraminifera in Pleistocene/Holocene sands on mid-Atlantic continental shelf: AAPG Bulletin, v. 68, p. 521.

Riggs, S. R., Snyder, S. W. P., Hine, A. C., Snyder, S. W., Ellington, M. D., and Mallette, P. M., 1985, Geologic framework of phosphate resources in Onslow Bay, North Carolina continental shelf: Economic Geology, v. 80, p. 716-738.

Riggs, S. R., Snyder, S. W., Ames, D., and Stille, P., 1999, Chronostratigraphy of the upper Cenozoic phosphorites on the North Carolina continental margin and oceanographic implications for phosphogenesis: *in* Marine authigenesis; from global to microbial, Glenn, C., et al. (eds.), Society of Economic Paleontologists and Mineralogists, Special Publication No. 66, p. 379-396.

Snyder, S. W., Mallette, P. M., Snyder, St. W., Hine, A. C., and Riggs, S. R., 1988, Overview of seismic stratigraphy and lithofacies relationships in Pungo River Formation sediments of Onslow Bay, North Carolina Continental Shelf: *in* Micropaleontology of Miocene Sediments in the Shallow Subsurface of Onslow Bay, North Carolina Continental Shelf, Snyder, S. W. (ed.), Cushman Foundation for Foraminiferal Research, Special Publication No. 25, p. 1-14.

APPENDIX A. FORAMINIFERA CLEANING PROCEDURE

Original version developed by P. Rosener, updated by E. A. Boyle (Boyle, pers. comm..); modified for PIXE use in this study.

FORAMINIFERA CLEANING PROCEDURE

Picking and weighing

- Pick sample tests with fine, sable-hair brush and deionizied water (dH_2O) in standard black boat
- Using forceps, weigh and tare out combusted-aluminum weigh boats for each sample
- Record test count and transfer tests to weigh boat
- Using forceps, weigh samples on microbalance; record weight
- Clean and destatic microscope platform, glass slides and black boat
- In black boat under magnification, transfer individual tests to glass slide and cover with another glass slide
- Crush samples by applying force equally to top plate, just until all chambers are opened
- Knock fragments into clean, dry, labeled 0.5 ml polypropylene microcentrifuge tube; sweep after if necessary with clean sable-hair brush
- Cap tubes and place in rack

Removal of fine clays

- Squirt a small amount of dH_2O into each tube, agitating the sample; rap the rack of tubes to remove bubbles
- Ultrasonicate for 1-2 minutes
- Repeat dH_2O agitation; rap to resettle fragments
- Allow to settle for 2-4 minutes; rap again, gently
- Using a 200 ul pipette tip on an Oxford micropipette, siphon off dH_2O to nearly the bottom of the tube, avoiding fragments
- Add 200 ul of glass-distilled methanol, rap and let resettle, siphon off carefully (methanol is less viscous, use caution)
- Repeat dH_2O/methanol process 2x more
- Rinse 2-3 times with dH_2O

Reducing reagent (to remove metal oxides)

- *Solution*: Mix 25 g citric acid into 500 ml reagent-grade ammonia **in an ice bath**
- *Reagent*: **In a fume hood**, add 750 ul of anhydrous hydrazine (caution: volatile, toxic and explosive!) to 10 ml ammonium hydroxide and 10 ml of *Solution*
- Add 100 ul of *Reagent* to each tube, using a 200 ul pipette tip on an Oxford micropipette; for small samples (<0.5 mg) add only 25 ul of *Reagent*
- Cap tightly (*Reagent* has high vapor pressure), return tubes to rack
- Cover rack with flat cover (plexiglass sheet) and tie to rack using ty-wraps to keep tubes capped
- Put rack in hot-water bath (80-90C) for 30 minutes, ultrasonicate about every 2 minutes
- **In a fume hood**, remove ty-wraps, uncap tubes and siphon off *Reagent*
- Add dH_2O to rinse (squirt to agitate sample), allow to settle; siphon off
- Repeat dH_2O rinsing 3x
- Fill tubes halfway with dH_2O
- Put rack in hot water bath for 5 minutes, ultrasonicate briefly

- Siphon off water
- Repeat dH_2O rinse, 5-minute hot water bath, and ultrasonication 1x

Oxidizing reagent

- *Reagent:* Mix 100 ul H_2O_2 (30% strength reagent-grade) to ~30 ml of 0.1N NaOH
- Add 250 ul of *Reagent* to each tube using a 1000 ul pipette tip on an Oxford micropipette
- Set in hot water bath for 5 minutes, ultrasonicate briefly, repeat 1x
- Squirt in dH_2O to agitate, rinse tube caps as well; rap and let settle
- Siphon off liquid
- Repeat dH_2O rinse 2x to insure all *Reagent* is flushed

Sample transfer

- Set up new, labeled microcentrifuge tubes in rack
- Cut ends of 200 ul pipette tips at an angle to produce a larger hole (use clean sharp straight razor); rinse cut tips
- Suck up fragments and remaining dH_2O with cut tip on an Oxford micropipette, expel into new, labeled tube
- Rinse evacuated tube with dH_2O; siphon off and expel into new tube
- Repeat rinse 1x; siphon off dH_2O

Weak acid leach

- Add 250 ul of 0.001 HNO3 to each tube using a 1000 ul pipette tip on an Oxford micropipette; let settle
- For small samples (<0.5 mg), siphon off acid and fill tube with dH_2O; let settle
- For larger samples, ultrasonicate 30 seconds, let settle 1 minute; siphon off
- Repeat acid leach 0-4x depending on size of sample; check sample each time
- After leaching, fill tubes with dH_2O, let settle; siphon off
- Samples can be stored indefinitely at this point

Sample dissolution

- Add 75 ul (40 ul for small samples) of 0.075N HNO3 (3x distilled) to each tube and cap
- Ultrasonicate to speed dissolution 15 minutes, rap to remove bubbles after 5 minutes
- Check for dissolution
- If necessary, add additional acid (record addition in lab book) and ultrasonicate
- Pipette a tiny amount of sample onto a strip of pH paper – a pH<4 indicates total dissolution
- Allow samples to settle and retest for pH; add more acid if necessary
- When all samples are dissolved, centrifuge for 5 minutes (0.5 ml tubes fit into 1.5 ml tubes for microcentrifuge)

APPENDIX B. TYPICAL GUPIX OUTPUT FORM

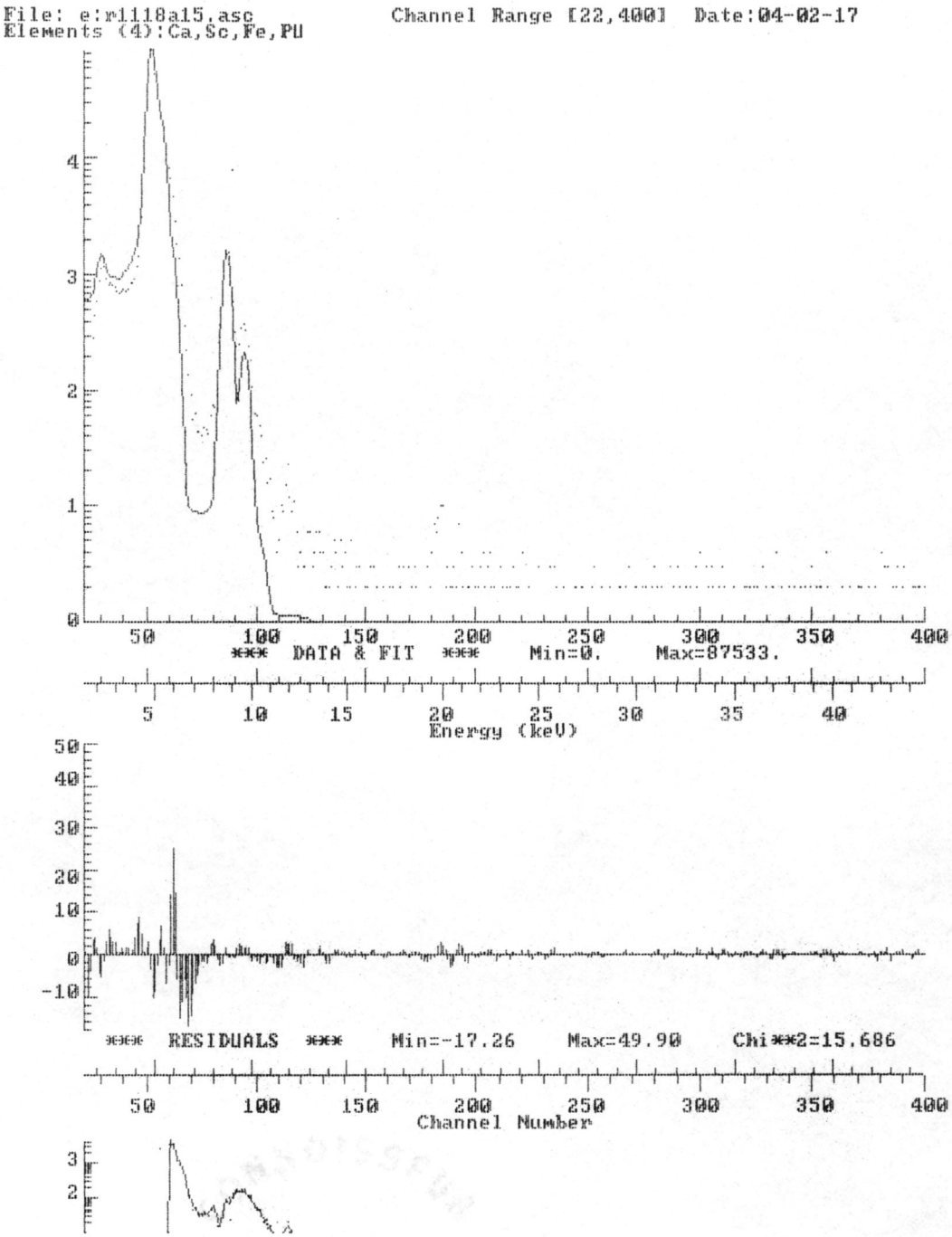
File: e:r1118a15.asc
Channel Range [22,400] Date:04-02-17
Elements (4):Ca,Sc,Fe,Pu
DATA & FIT
Min=0.
Max=87533.
Energy (keV)
RESIDUALS
Min=-17.26
Max=49.90
Chi**2=15.686
Channel Number

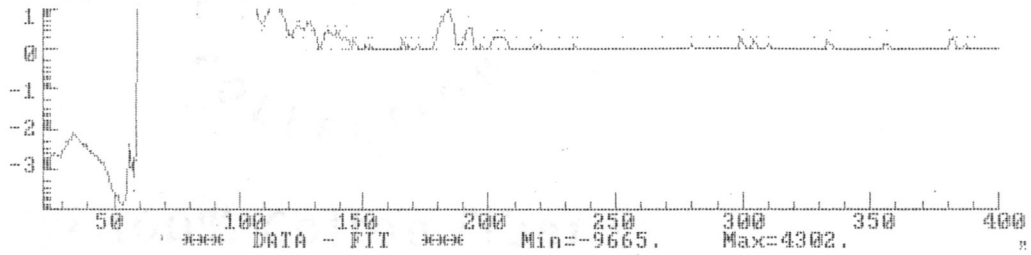


```
        ***  GUPIX - Guelph Thin/Thick/Layered Target PIXE Program  ***
                          GUPIX98  Last Update: 99-01-15
Time: 15:35:17                  *** Results ***              Date (y-m-d): 04-02-17

File:e:r1118a15.asc (AP0PAR.VAL) ID: Elec 002                          Type:Ox Asc
Chi**2= 15.69       ( 45.37     )  Total counts:  478923  %RMS sys err= 10.65
Total # of loops:   1                    Total fit time:    0.2 seconds.
Fit region has  379 chan (  22 to  400).  File has 2048 chan with offset    1
The detector resolution at the 5.9 keV line is  325.9 eV   (160.)
Case: Thick PIXE    Acquisition date,time(**- 1-** @ 17:27) Duration:   1200s.
    (Trace)    Average count rate(cps):   399.1   Average current(nA):   0.000
H: 2.400E+03                             Angle(Beam-Target normal) Alpha=  0
Charge: 8.716E-05                        (Detector- "     "   ) Theta= 45
  Proton energy(keV): 2020  Exit keV: 2010  Layer thickness(ug/cm2): 7.968E+01
Depth fraction:0.000              Density(gm/cm3): 0.000
Matrix ( 3) elmts (Z,ppt): ( 6, 120.0) ( 8, 479.6) (20, 400.4)
Looking for  3 elmts:  Ca K , Sc K , Fe K
Filters (Z,um,hole fraction):                  Fractional absorber error:0.010
(104,   79.00,0.00)
(100:Mylar, 101:Acrylic, 102:Air, 103:Ice, 104:Polyethylene, 105:Kapton)
Detector efficiency correction of relative intensities:  On
Det #,Be,Au,Si,Distance(cm):  1, 1.27E-03, 2.00E-06, 0.557,  5.20
Ag/At par: 1.840 Det Res(eV):160. Tau(ns): 500.  Zs: 47914.  Deadtime(us): 25.0
Ag/At par is energy cutoff in keV
Det ID: Ortec (Uncollimated)

        Peak and spectrum description:
Peak centroid = A1+A2*E+A3*E**2            A(1,2,3):    3.954   13.530 -0.1045
Peak width = SQRT(A4+A5*E)                   A(4,5):   2.3707   0.0894
With these values the fit region extends from   1.35 to   44.70 keV with FWHM
at center being  568.2 eV or  4.95 channels.  Excluding pile-up & escape the
elements have peaks ranging from   3.647 to   7.129 keV.

Background handled by User (Constant) digital filter (m-n-m): ( 2- 4- 2)
Basic peak shape: Gaussian below & Voigtian above peak heights = 1000
Peak plateau: Energy dependent parameterized plateau in use.
Short step: None.
Peak tailing: 2 energy dependent parameterized tails per peak.
Matrix abs. edges: None.
Si escape energy in keV:  1.742
Minimum background value for LOD calc:    1
Statistical + Systematic channel weighting used -
    Rel.Int. error:0.010              Absorber error:0.010
    KMM R.A. error in use ? T         Tail error in use ? F
Pile-up [99(PU S )] peaks - #allowed:  3,  #used:  3

Stopping criteria: STEP:0.0010    LOOPS:  20
Total # of pars., fixed pars. & their IDs: ( 9, 0)
################################################################################
 Note: ID/n,  n:(-2:filter, -1:surface, n:layer number)
 #    ID      FINAL VALUE   INIT. VALUE      ERROR     %ERROR LAST CHANGE   %CHANGE
 -    --      -----------   -----------      -----     ------ -----------   -------
 1              3.95390       3.98770      6.346E-04     0.02  -1.895E-04      0.00
 2              13.5295       13.5156      1.531E-04     0.00  -4.297E-05      0.00
 3             -0.104451     -0.103595     3.240E-05    -0.03  -7.510E-06      0.01
 4              2.37066       2.17417      1.740E-03     0.07  -1.911E-04     -0.01
 5             8.944373E-02 0.141414       4.354E-04     0.49  -6.184E-05     -0.07
 6 Ca K / 1    58566.2       83003.0       632.          1.08   4.879E+03      8.33
 7 Sc K / 1    6150.68       14411.0       162.          2.63   -187.         -3.04
 8 Fe K / 1    1040.53       1654.00       21.0          2.02    1.25          0.12
 9 PU S1/ 0    6.53100       10.0000       8.07        123.62  -0.697        -10.67
################################################################################
     Elmt  Lay   DF     Peak     2-FWHM        % Fit  % Stat. +1% Of      LOD
```

```
 #    Z Sym.      n/m     Area        Area        Error    Error Overlap     Area
 -    - ----      ---     ----        ----        -----    ----- -------     ----
 1: 20 CaK / 1   4/ 2  2.4126E+05 4.0291E+05     1.08     0.18     0.21    602.5
 2: 21 ScK / 1   4/ 2  2.5504E+04 4.1605E+04     2.63     1.30     5.50   2612.4
 3: 26 FeK / 1   4/ 2   4475.      6788.         2.02     1.36     1.36     50.8
################################################################################
Z=99 is a pile-up "element".  Up to  3 such peaks were allowed in the fit and
the program used  3 of them.  Below are listed the pile-up energies and
intensities.   (Total Cts:   478923  Live time: 1188.0s   Av Rate:   403 cps)
 (Tau:  500. ns,   Pulse deadtime: 25. us, % Live time:  99.0  PUcor: 1.0004 )
Energy:   7.381  7.702  7.780
Rel Int: 1.0000 0.2614 0.2116
################################################################################
File:e:r1118a15.asc           Sec: 1200.  uC:  0.000  nA:  0.000  PUcor:1.0004
The last column is a decision on the presence of that element in the spectrum.
(A "*" indicates the minimum background was used in the LOD calc).
  Y: present at level of quantization,   N: not present at limit of detection
  ?: may be present near LOD levels (user must decide)      H or uC Corr: 1.00
Note: Surface element (Layer=-1) concs in ng/cm2            Det Res(eV):325.9
      Layer          H    Yield Det. Filter          Chi**2:   15.686 (   45.368)
Element     Area  value  /uC/ Eff. Trans.     Conc.  %Stat.  %Fit      LOD
 Z Sym   #  counts (  0)   ppm (-3)  (-5)      ppm    Error  Error     ppm
 - ---   -  ------ -----  ---- ---- ------    -----   -----  -----    -----  -
20 CaK   1  241261  2400 109.8  853  74066  16642.6    0.21   1.08     30.7  Y
21 ScK   1 25504.4  2400 77.96  884  80327   2202.5    5.50   2.63    169.7  Y
26 FeK   1  4474.9  2400 21.23  960  94668   1109.1    1.36   2.02      9.8  Y
################################################################################
```

APPENDIX C. PIXE ACCELERATOR PARAMETERS AND GUPIX ANALYSES RESULTS

Appendix C-a. PIXE accelerator parameters and GUPIX analyses results for *1006* analysis (October 6, 2003); cps = x-ray counts per second, I = beam intensity in nannoamps.

run #	cps	I	CORE #	Ca	Fe	Fe/Ca	Sc	Sc/Ca	Zn	Zn/Ca
17	429	1.25	**OB-16**	631.8	14.1	0.0223	41.3	0.0654		
24	440	2.35	**OB-107**	672.7	9.8	0.0146	67.5	0.1003		
3	406	3.20	**OB-30**	644.0	6.9	0.0107	95.0	0.1475		
15	178	1.30	**OB-24**	266.7	14.4	0.0540	20.0	0.0750		
2	286	7.20	**OB-66**	447.7	14.6	0.0326	56.5	0.1262	4.9	0.0109
16	426	1.25	**OB-62**	639.7	41.6	0.0650	53.1	0.0830		
4	309	1.50	**OB-127**	501.4			68.8	0.1372		
19	372	0.70	**OB-70**	569.9	7.3	0.0128	52.9	0.0928		
13	404	2.05	**OB-25**	612.2	16.9	0.0276	43.6	0.0712		
18	355	0.80	**OB-115**	505.6	46.0	0.0910	26.6	0.0526		
5	237	1.60	**OB-29**	350.9	23.0	0.0655	26.3	0.0750		
14	489	1.00	**OB-98**	745.5	17.8	0.0239	64.9	0.0871		

12	24	6.50		U	25.6	0.84	0.0327		0.0000		
21	342	0.35	**OB-70c**	P	521.6	9.0	0.0173	50.3	0.0964		
9	560	0.65		A	847.4	18.8	0.0222	71.1	0.0839		
6	337	1.00		U	523.3	1.4	0.0027	53.2	0.1017		
7	436	1.00	**OB-24c**	P	675.8	18.5	0.0274	63.9	0.0946		
8	259	1.00		A	383.6	39.6	0.1032	27.6	0.0719		
20	266	0.25		U	417.1		0.0000	41.9	0.1005		
10	8	6.20	**OB-127c**	P	3.8		0.0000		0.0000		
11	146	6.40		A	202.7	9.5	0.0469	8.9	0.0439		

elemental concentrations in ng/cm^2

U = unaltered, P = partially altered, A = altered

10-15% fit error

not present

Appendix C-b. PIXE accelerator parameters and GUPIX analyses results for *1013* analysis (October 13, 2003); cps = x-ray counts per second, I = beam intensity in nannoamps.

run #	cps	I	CORE #		Ca	Fe	Fe/Ca	Zn	Zn/Ca	Sr	Sr/Ca	Mn	Mn/Ca	Sc	Co	Cu
21	298	8.0	**OB-16**		243890276.7	5585291.6	0.0229	20.4	8.35E-08	90.3	3.70E-07	139.9	5.74E-07			
2	280	12.5	**OB-107**		230762945.0	2951648.3	0.0128	46.2	2.00E-07	80.3	3.48E-07		0.0000	573947.9		
6	282	17.5	**OB-30**		229132074.7	1409060.7	0.0061	42.3	1.85E-07	101.8	4.44E-07		0.0000			
19	289	8.0	**OB-24**		231121062.0	7934311.7	0.0343	40.2	1.74E-07	66.0	2.86E-07		0.0000			
1	263	15.0	**OB-66**		206702289.7	5432438.4	0.0263	109.6	5.30E-07	66.0	3.19E-07		0.0000			
20	291	5.0	**OB-62**		211148692.3	19695224.6	0.0933	28.7	1.36E-07	73.6	3.49E-07		0.0000			
7	365	16.5	**OB-127**		309396689.7	671148.6	0.0022	52.3	1.69E-07	130.0	4.20E-07		0.0000			
23	305	3.5	**OB-70**		253098492.8	3585901.3	0.0142		0.0000	105.5	4.17E-07	166.4	6.58E-07			
16	308	8.0	**OB-25**		250230799.1	6261711.0	0.0250	29.1	1.16E-07	94.1	3.76E-07	129.7	5.18E-07			
22	306	11.5	**OB-115**		215472019.3	24792088.7	0.1151	58.5	2.72E-07	77.9	3.61E-07	215.9	1.00E-06			
8	245	18.5	**OB-29**		184320253.6	11625629.0	0.0631	64.2	3.48E-07	62.7	3.40E-07		0.0000			
17	310	15.1	**OB-98**		251753170.6	7486293.7	0.0297	30.7	1.22E-07	91.3	3.63E-07	165.8	6.59E-07			
15	311	12.5		U	258888484.1	1398519.1	0.0054	99.4	3.84E-07	108.3	4.18E-07	140.5	5.43E-07			
25	292	4.0	**OB-70c**	P	242908902.2	3944315.7	0.0162	29.4	1.21E-07	111.1	4.57E-07	124.2	5.11E-07			
12	280	10.0		A	225054662.6	3747539.2	0.0167	13.4	5.98E-08	63.4	2.82E-07	135.7	6.03E-07			
9	304	13.5		U	253095813.8	316248.0	0.0012	20.0	7.90E-08	95.9	3.79E-07	76.6	3.03E-07			
10	340	11.0	**OB-24c**	P	278704527.3	1969522.5	0.0071	14.9	5.35E-08	87.6	3.14E-07	130.9	4.70E-07			
11	292	15.0		A	194080103.8	2641549.5	0.0136	66.9	3.45E-07	50.9	2.63E-07	180.9	9.32E-07		269.3	65.7
24	330	7.0		U	281666536.9	630739.1	0.0022	38.2	1.35E-07	102.9	3.65E-07		0.0000			
13	323	13.0	**OB-127c**	P	259721647.9	4634790.6	0.0178	34.9	1.34E-07	76.1	2.93E-07		0.0000			
14	297	12.0		A	222845604.7	11572921.0	0.0519	86.1	3.87E-07	99.7	4.47E-07	290.1	1.30E-06			

elemental concentrations in ng/cm^2

U = unaltered, P = partially altered, A = altered

10-15% fit error

not present

Appendix C-c. PIXE accelerator parameters and GUPIX analyses results for *1118* analysis (November 18, 2003); cps = x-ray counts per second, I = beam intensity in nannoamps.

run #	cps	I	CORE #	Ca	Fe	Fe/Ca	Sc	Sc/Ca	Zn	Mn	Co
16	363	1.50	**OB-16**	1167.3	42.6	0.0365	169.0	0.1448		6.4	10.5
6	240	1.45	**OB-107**	725.3	12.2	0.0168	94.5	0.1303			
7	226	1.40	**OB-30**	693.3	5.1	0.0074	93.6	0.1350			
14	323	1.45	**OB-24**	1019.4	22.4	0.0220	145.5	0.1427			
19	313	1.50	**OB-66**	1004.0	26.4	0.0263	135.0	0.1345	8.9		
15	399	1.50	**OB-62**	1309.3	89.0	0.0680	171.1	0.1307			
8	375	1.35	**OB-127**	1263.0		0.0000	193.4	0.1531			
18	459	1.50	**OB-70**	1766.0	49.3	0.0279	270.4	0.1531		7.9	15.6
12	349	1.50	**OB-25**	1127.0	32.0	0.0284	158.3	0.1405			9.6
17	373	1.50	**OB-115**	1187.9	117.2	0.0987	150.3	0.1265			
9	315	1.35	**OB-29**	994.5	65.9	0.0663	127.8	0.1285	4.7		
13	396	1.45	**OB-98**	1303.1	38.8	0.0298	194.5	0.1493			

elemental concentrations in ng/cm^2

10-15% fit error

not present

APPENDIX D. PREVIOUSLY PUBLISHED GEOCHEMICAL DATA

Appendix D-a. Inductively Coupled Plasma-Optical Emission Spectrometry (ICP) of phosphate grains from Frying Pan phosphate district (Ellington, 1984).

Core	Depth	Unit	Morphology	P_2O_5	Fe_2O_3
OB-24	0.3-0.5	FPS-1	pellet	28.5	0.48
OB-24	0.3-0.5	FPS-1	intraclast	28.2	0.63
OB-24	0.3-1.5	FPS-1	pellet	28.6	0.45
OB-24	0.3-1.5	FPS-1	pellet	28.8	0.49
OB-24	0.3-1.5	FPS-1	pellet	28.4	0.49
OB-24	0.3-1.5	FPS-1	intraclast	27.2	0.93
OB-24	0.3-1.5	FPS-1	intraclast	27.5	0.96
OB-24	0.3-1.5	FPS-1	intraclast	24.9	0.71
OB-24	0.75-1.5	FPS-1	microsphorite	20.0	1.17
OB-24	0.75-1.5	FPS-1	microsphorite	22.5	0.53
OB-24	0.75-1.5	FPS-1	skeletal	32.4	0.24
OB-24	0.75-1.5	FPS-1	intraclast	27.1	0.82
OB-24	0.75-1.5	FPS-1	pellet	30.2	0.52
OB-24	1.5-1.67	FPS-1	skeletal	31.1	0.24
OB-24	1.5-1.67	FPS-1	pellet	27.9	0.44
OB-24	1.5-1.67	FPS-1	pellet	28.9	0.48
OB-24	1.7-2.7	FPS-1	microsphorite	21.8	0.55
OB-25	0.5-0.5	H	pellet	27.9	1.14
OB-25	1.25-1.5	FPS-1	pellet	28.3	0.62
OB-29	1.25-1.5	FPS-1	pellet	29.3	0.76
OB-29	7.0-7.21	FPS-1	skeletal	30.6	0.27
OB-29	7.0-7.20	FPS-1	intraclast	29.9	0.41
OB-29	7.0-7.20	FPS-1	pellet	28.5	0.40
OB-30	1.50-1.50	FPS-1	pellet	28.5	0.37

Appendix D-b. Inductively Coupled Argon Plasma Emission Spectrometry (ICAPES) of bulk sediment samples from Frying Pan phosphate district (Mallette, 1986).

Core	depth	seismic unit	P_2O_5	Fe_2O_3
OB-16	0.50-0.75	u	0.88	4.78
OB-16	4.25-4.50	u	0.84	5.00
OB-16	5.75-5.82	u	1.21	5.27
OB-24	0.30-0.50	FPS-1	9.26	0.99
OB-24	1.00-1.25	FPS-1	23.20	0.58
OB-29B	0.25-0.50	FPS-2	0.77	0.34
OB-29B	3.00-3.25	FPS-2	3.42	1.51
OB-29B	6.00-6.25	FPS-1	6.94	0.98
OB-62	3.25-3.50	u	1.60	2.77
OB-62	4.25-4.50	u	1.69	3.16
OB-62	5.75-5.82	u	1.93	3.11
OB-66	3.50-3.60	FPS-3	1.77	1.65
OB-98	1.25-1.50	FPS-2	1.53	2.86
OB-98	1.40-1.50	FPS-2	1.25	2.82
OB-98	3.25-3.50	FPS-2	1.02	2.87
OB-98	4.00-4.10	FPS-2	1.00	3.48
OB-107	0.50-0.75	FPS-6	1.19	4.24
OB-107	1.50-1.75	FPS-6	1.30	4.80
OB-107	2.50-2.75	FPS-6	1.46	4.54
OB-127	1.50-1.75	FPS-1	11.40	1.48
OB-127	3.50-3.75	FPS-1	8.37	1.14
OB-127	5.50-5.75	FPS-1	2.31	1.88
OB-127	7.50-7.75	FPS-1	1.45	1.12

Appendix D-c. Geochemical analysis of bulk sediments and phosphate concentrates from FPS-1 and FPH (Riggs et al., 1995).

	SAMPLE	n =	P_2O_5	Fe_2O_3
total sediment	FPS-1	34	12.4	0.63
	FPH	53	6.3	1.30

standard wet chemical analysis (Assoc. Florida Phosp. Chem.)

	SAMPLE	n =	P_2O_5	Fe_2O_3
phosphate concentrate	FPS-1	10	29.3	0.41
	FPH	7	26.5	1.46

standard metallurgical and wet chemical analysis (Assoc. Florida Phosp. Chem.)

	SAMPLE	n =	P_2O_5	Fe_2O_3
handpicked phosphate concentrate	FPS-1	25	28.69	0.518
	FPH	11	28.50	1.45

inductively coupled argon plasma emission spectroscopy (ICAPES)